CFD based Hydrodynamic Optimization and Structural Analysis of the Hybrid Ship Hull

Kandasamy, M.[1], Wu, P.C.[1], Zalek, S.[2], Karr, D.[2], Bartlett, S.[3], Nguyen, L. [3], and Stern, F.[1]
[1] University of Iowa
[2] University of Michigan
[3] NSWC, Carderock Division

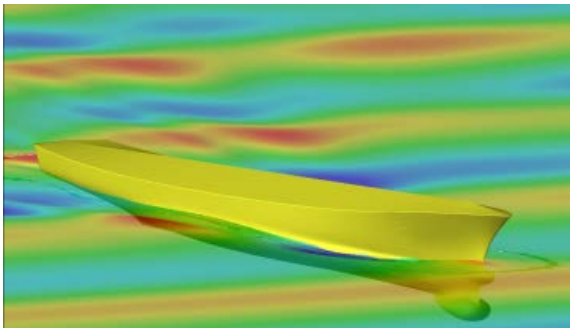

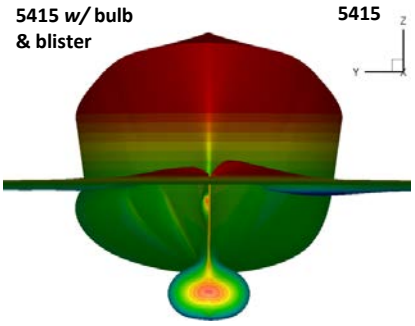

The US Navy is currently considering the introduction of a Flight III variant beginning with DDG-123 in Fiscal Year 2016. The new design incorporates a new combat system and associated power and cooling upgrades. The overall system improvements increase the payload of the ship and the resulting increased displacement has a negative impact on the service life allowance for range, fuel consumption and sea-keeping characteristics. The present objective is to increase the hull displacement without resistance and sea-keeping penalty and with minimal modifications to the baseline DTMB-5415 design (open literature surrogate of the existing DDG-51 hull form) by using retrofitted blisters in the form of side hull expansions and a bow-bulb. The investigation makes use of high-performance CFD computing for analysis of wave cancellation mechanisms, reduced order, rapid hydrodynamic analysis codes, general purpose finite element modeling and structural integrity analysis, sea-keeping evaluation for cost and performance tradeoffs, geometric sensitivity studies and multi-objective optimization. A candidate modified 5415 design with both blisters and bow bulb shows a resistance reduction of ~11% w.r.t. the baseline 5415 in the design speed range of 15-19 knots, even though the displacement is increased by 8%, such that the transport factor is increased by 19%.

KEY WORDS: Wave-cancellation; side-hull blisters, bow-bulb; hybrid ship; multi-objective optimization; high-performance computing; simulation-based design

1. INTRODUCTION

The US Navy is currently considering the introduction of a USS Arleigh Burke-class destroyer (DDG-51) Flight III variant (Fig. 1) beginning with DDG-123 in FY16. The new design incorporates a new combat system and associated power and cooling upgrades. The overall system improvements are expected to increase the payload of the ship by approximately 500 tons (distributed between the topside arrays and the below deck power and cooling systems). This increased displacement has a negative impact on the service life allowance for range, fuel consumption and sea-keeping characteristics. Without changes to the hull form, the increased displacement will also reduce the hydrodynamic efficiency of the hull leading to an increase in annual fuel costs.

Fig. 1 DDG-51 Flight III Variant (Vandroff, 2013)

The purpose of this study is to investigate concept designs that could accommodate the increase in displacement with minimum resistance and cost penalties. The research was conducted as a collaborative team effort guided by NSWC/Carderock Divison whereby hydrodynamic optimization was conducted using both Unsteady Reynolds Averaged Navier-Stokes (URANS) and potential flow solvers at University of Iowa and University of

Michigan, respectively, and structural analyses were conducted at the University of Michigan.

Several simulation-based design tools that have previously been successfully implemented for a variety of design optimization problems were used. The first phase investigated the initial concepts provided from the concept definition and mission requirement stage, which included both flared and wave piercing hull types. The initial design objectives were unconstrained and a large design envelope was explored, including modifications to the bow, blisters, and stern.

The CFD hydrodynamic investigation focused on the interaction between the free-surface wave and the blister. A shoulder wave cancellation mechanism was identified which allowed for progressive analysis of geometry variations for best design variables capable of producing destructive interference of the diverging Kelvin wave. The resulting geometry indicated that a reduced resistance was possible even with an increase in displacement through calculated shaping of the blister for shoulder wave cancellation, thus provided a proof-of-concept.

The second phase was initiated to build upon the proof-of-concept. The initial plan was to include cargo boxes at the side hulls such that the side hull expansions reach the deck, thus increasing the hull beam. During the course of the project, this design was deemed unfeasible due to material cost and sea-keeping considerations. Hence, the concept definition and mission requirement were modified such that the blisters were required only to increase the ship displacement and not hold cargo. Designs for submerged-blisters for sea-keeping considerations and incremental-blisters for multiple speed operations were examined. The new concepts allowed for the same water-plane area and draft as the original-5415, notwithstanding the added displacement.

Previous studies on DDG-51 modernization have focused on the design of bow-bulbs for resistance reduction without taking into consideration any increase in displacement. Cusanelli and Karafiath, (1994) designed a bow-bulb concept, retrofitted above the pre-existing sonar dome, that improved the resistance characteristics over the entire operational range in both calm water and rough seas. During the current study, a similar bow-bulb was designed and optimized along with the blisters to investigate the effects of both the bow-bulb and the blisters functioning together. The combined blister and bow-bulb concept designs show promise for significant performance improvements.

2. CONCEPT DEFINITIONS

2.1. Phase I

The initial concept definition stage provided six feasible variants of the baseline DTMB 5415 (as surrogate for DDG-51) with flared and wave piercing bow. Fig 2 has been extracted from Barsoum (2013) and shows the different hull forms including the flared and wave-piercing bow of the proposed hybrid hull concepts. Critical issues in material processing and structural behavior that must be taken into account to maximize hybrid hull performance are discussed in detail in Shkolnikov (2014).

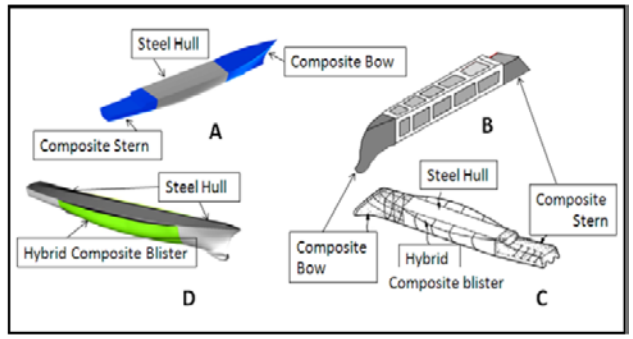

Fig. 2 Hybrid ship concepts

Hybrid hull Type A has composite bow and stern; and Type B has composite bow and stern and the mid-section is made of steel framing and composite panels (Barsoum 2005). Type C has composite bow and stern, while the mid-section is a conventional steel hull with composite side expansions (or blisters). For sake of weight reduction, these side expansions are constructed of steel framing with composite panels. Hybrid hull D, is similar to C, except that the hull is the original steel baseline, including bow and stern, while the side expansion blisters are hybrid steel framing with composite panels. The use of composites in hybrid ship hull allows for complex shapes that can be easily manufactured with high precision based on optimized complex shapes to achieve improved hydrodynamic performance in addition to other desired improvements.

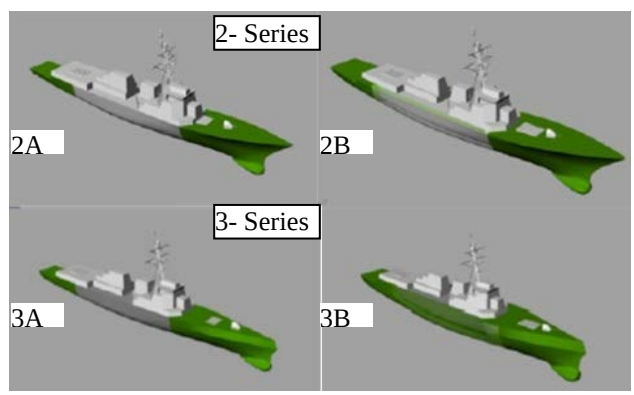

Fig. 3 Initial concept design variants

The flared hull variants (2-series) included (1) 5415-variant 1, which is the steel baseline, (2) 2A, which has composite flared bow and composite transom attached to the steel core mid-section, (3) 2B, which has composite flared bow, transom, and blisters attached to the steel core mid-section, and (4) 2C, which has only composite blisters attached to the steel baseline. Similarly, the bow piercing hull variants (3-series) included (1) 3A, which has composite wave-piercing bow and

composite transom attached to the steel core mid-section, (2) 3B, which has composite wave-piercing bow, transom, and blisters attached to the steel core mid-section, and (3) 3C, which has only composite blisters attached to the steel baseline. Fig. 3 illustrates the variants.

2.2. Phase II

Since the initial blister designs decreased the roll period substantially, a paradigm change had to be implemented to the hybrid concept design. The blisters were modified to be entirely submerged, while keeping most of the wave-cancellation design features intact, so that the water-plane area does not increase. DTMB-5415 geometry was selected for the optimization problem instead of the DDG-51 variants, since it facilitates validation of the blister design by appending it to pre-existing *INSEAN* DTMB-5415 geometry. Also, extensive CFD and model testing data for resistance and sea-keeping is already available for DTMB-5415. The modified blister displacement criteria based on new information of the added weights require 8% increase in displacement *w.r.t.* the original 5415 hull. Static draft constraints were also imposed to minimize structural modifications to the original 5415 hull. Initial submerged blister designs were generated by replicating the design features of the Phase I optimized ship as best as possible, while subject to the new geometry criteria.

3. CFDSHIP HYDRODYNAMIC OPTIMIZATION STUDIES

3.1. Simulation based design framework

The toolbox used by the University of Iowa for the optimization is a product of the long-term ongoing collaboration between *IIHR*, *INSEAN*, and *NMRI* research groups. The toolbox consists of the high fidelity (*HF*) *URANS* solver CFDShip (Huang *et al.*, 2008), and the low fidelity (*LF*) linearized potential flow solver *WARP*, two evolutionary optimization algorithms, namely a multi-objective genetic algorithms - *MOGA* (Tahara *et al.*, 2008) and a particle swarm optimization (*PSO*) method (Campana *et al.* 2009). It also contains different geometry modification tools. Previous versions of the toolbox have been successfully used for progressively complex designs, namely, mono-hull surface combatant (Campana *et al.* 2006), multi-hull high speed sea lifts (Tahara *et al.*, 2008), *SWATH* displacement ships (Stern *et al.*, 2008), foil-assisted semi-planing catamaran ferries (Kandasamy *et al.*, 2011a) and barehull and *WJ* inlet optimization of Delft Catamaran (Kandasamy *et al.*, 2013). The current study extends the Simulation Based Design (*SBD)* toolbox to the optimization of the hybrid ship concept.

3.1.1. CFDShip

The high-fidelity solver used for the analysis was CFDShip v4.5, which is a general purpose hydrodynamic solver developed for ship hydrodynamics applications. For the current simulations, URANS with the shear-stress transport turbulence model was used. The free surface location is predicted by a single phase level set method. A finite difference second order upwind scheme is used to discretize the convective terms of the momentum equations for URANS and solved using the predictor-corrector method. A projection method is used to enforce mass conservation on the collocated grids. The pressure Poisson equation is solved using the PETSc toolkit. All the other systems are solved using an alternating direction implicit (ADI) method. A MPI-based domain decomposition approach is used, where each decomposed block is mapped to one processor. The software SUGGAR runs as a separate process from the flow solver to compute interpolation coefficients for the overset grids and communicates with a motion controller (6DOF) within CFDShip at every time-step. The software USURP is used to compute area and forces on the surface overlap regions.

3.1.2. Geometry modification

Tools for geometry modeling (and its necessary sequel, the automatic grid deformation) are another relevant SBD component. An efficient and flexible way to modify the geometry of the body is necessary for a full investigation of the design variables space and a successful optimization. Techniques should be versatile enough to describe a broad variety of complex 3D configurations and sufficiently compact to use as few variables as possible. Once the optimization algorithm obtains the vector with the new design variable values, the deformations are spread over the body surface and the computational volume grid. The deformation of the body is defined and controlled by using reduced control points, much less than the number of nodes used in the discretization adopted for the flow analysis.

The control points are modified by different methods. The first method is based on the use of Bezier polynomial patches. A Bezier patch is the surface extension of the Bezier curve. The geometry is modified by superimposing one or several Bezier surfaces onto the original ship geometry. Each Bezier patch is controlled by a given number of control points, p, that are used as design variables by the optimizer. The number and position of the patches and the number of control points per patch can be changed in an easy and flexible way, depending on the details of the assigned problem. At the junction between two patches continuity on the first and second derivative can be enforced to ensure the fairing of the body's surface. The second method is by using algebraic curves over a field of modification K using an equation $f(x, y) = 0$, where $f(x, y)$ is a polynomial in X and Y with coefficients in K. A point on an algebraic curve is simply a solution of the equation of the curve. A K-rational point is a point (x, y) on the curve, where X and Y are in the field of modification K. This allows for precise modification of the nodes through combination of equations representing different shapes such as tear-drop, hydrofoil, sigmoid, serpentine, deltoid etc.

3.2. Phase I Studies

3.2.1. Initial 5415 grid design

The URANS code CFDShip v4.5 was used for the resistance computations. The code was recently validated for 5415 in the Gothenburg '10 workshop. The finest grid used 20 million grid points and showed <5% error in resistance compared to the benchmark data over the Froude numbers 0.138< Fr < 0.41.

Typical ship optimization problems require hundreds of simulations to get the optimal design. Hence, a medium sized grid of 3 million points was constructed to keep run times manageable. The validation work for the Gothenburg 2010 workshop used 20 million grid points, and the same cases were simulated using the current 3 million point grid to assess accuracy. The main full scale particulars of the case validated are as follows: L_{WL} = 142.18 m, Draft = 6.15 m, Displacement = 8635 MT.

The results with 3 million grid points show good agreement with the EFD with errors 3.2%, -1.4% and -6.2% for Fr=0.138, 0.28 and 0.41, respectively. The sinkage and trim results deviate more from the experiments, but a higher error in sinkage and trim is normally expected at lower Fr since the values are small.

3.2.2. Evaluation of initial concepts

3.2.2.1 Calm-water resistance

Hybrid ship variants 2A and 3A have composite bow and stern and 2B and 3B have blisters included for increased displacement. To better compare the hydrodynamic performances, simulations for the variants were conducted at both displacements. Fig. 4 shows the relative displacements and the resistances of the different designs at 20 knots (Fr=0.28).

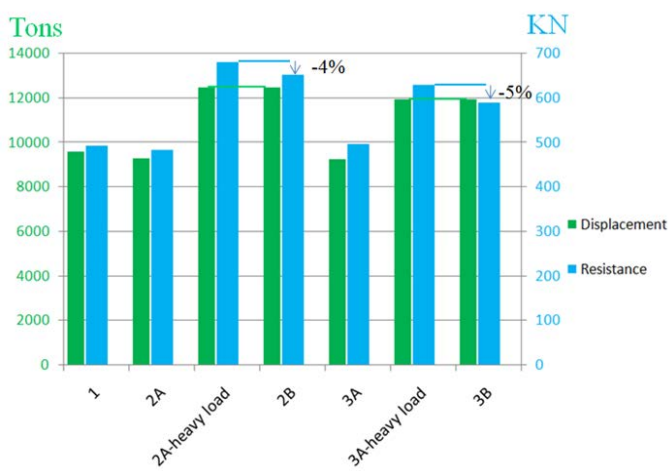

Fig. 4 Performance comparison of the initial concepts

Calm water resistance analysis (Fig. 5) indicates that the 2B and 3B blister concepts exhibited a decrease in resistance compared to 2A and 3A at heavy load conditions (to match 2B and 3B displacement) at design Fr=0.28, but showed an increase in resistance at Fr=0.41. The conflicting trend for Fr=0.28 and Fr=0.41 prompted investigation into the flow physics of the blister concepts. Analysis of the wave and volume flow solutions at design speed Fr=0.28 revealed that the blisters cancel the shoulder waves akin to a bulbous bow cancelling the bow wave, and the resulting phase-shift of the near-field wave system lead to better pressure recovery at the transom (Fig. 5).

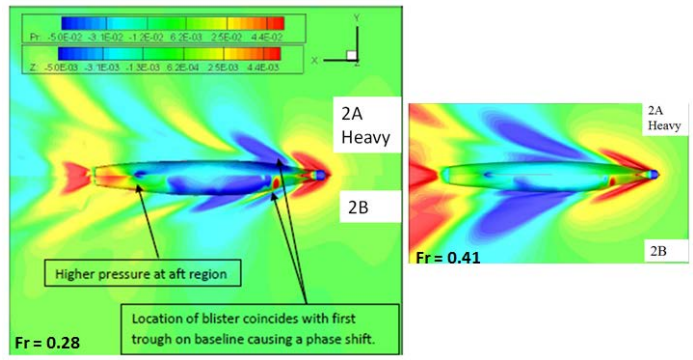

Fig. 5 Volume flow analysis of blistered *vs.* non-blistered designs for Fr=0.28 and Fr=0.41

However, at Fr=0.41 the location of the blister occurs within the bow wave, and hence it magnifies the wave elevations, with no beneficial phase shift.

3.2.2.2 Sea-keeping

Sea-keeping simulations were conducted for the hybrid ship variants 2A and 2B operating at Fr=0.28 in regular incoming waves of amplitude A/L=0.00625 and wavelength λ/L=1.5 at different headings. The heave, pitch and roll RAOs are tabulated in Table 1.

Table 1: Heave, pitch and roll RAOs

Geometry	0° Head waves T_e=7.47s			45° Bow waves T_e=8.36s			90° Beam waves T_e=11.74s		
	Heave	Pitch	Roll	Heave	Pitch	Roll	Heave	Pitch	Roll
2A	0.81	0.94	0.00	0.89	0.71	3.22	1.00	0.07	4.15
2B	0.97	1.02	0.00	0.95	0.76	5.83	0.95	0.11	2.70
% dif.	+20.2	+7.6		+6.5	+7.6	+81.0	-5.3	+72.4	-34.8

135° Quartering waves T_e=19.73s			180° Following waves T_e=27.51s		
Heave	Pitch	Roll	Heave	Pitch	Roll
0.65	0.48	1.64	0.56	0.58	0.00
0.64	0.46	1.20	0.60	0.58	0.00
-1.6	-4.3	-26.9	+7.1	+0.1	

The natural roll period for 2A and 2B are 13.16s and 8.03s, respectively. For head and following wave conditions, 2B had larger pitch and heave RAOs due to its larger frontal area. For oblique waves, the roll RAOs increased with the proximity of

the encounter frequency to the natural frequency of the ships. For λ/L=1.5, 45° bow waves correspond to an encounter frequency of 8.36s which is closer to the natural frequency of 2B that showed 81% larger roll RAO compared to 2A. Whereas, 90° beam waves correspond to an encounter frequency of 11.74s which is closer to the natural frequency of 5415-variant 1 which showed a 54% larger roll RAO compared to 2B.

3.3. Single speed design optimization for blisters, bow and stern

3.3.1. Sensitivity studies on blister location

The blister location was shifted both to the fore and the aft to evaluate the hydrodynamic effects. Fig. 6 shows the hull surface pressure for the different blister configurations, and the resistance change *w.r.t.* the baseline ship *w/o* blisters. The best resistance reduction is obtained when the blister leading edge coincides with the bow wave trough.

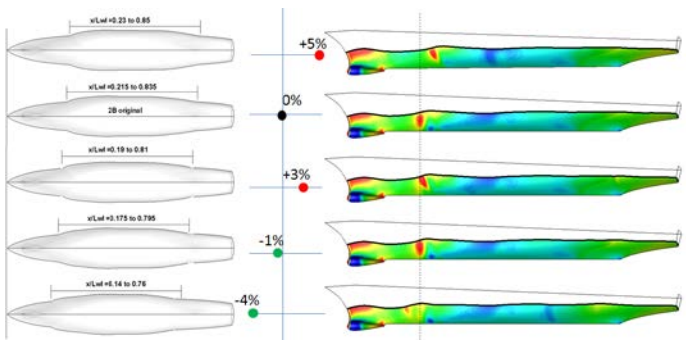

Fig. 6 Blister locations, resistance changes *w.r.t.* baseline, and surface pressure contours

3.3.2. Transom optimization

The stern was optimized for better pressure recovery and reduction of stern losses. Fig. 7 shows the stern geometry modification, which was carried out using b-splines. The pressure contours indicate a better pressure recovery at the transom for the best transom design.

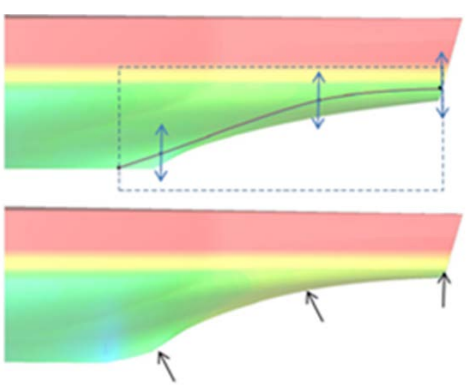

Fig. 7 Stern modified using 3 point b-splines

3.3.3. Initial Optimization

A particle swarm optimization was carried out by blending the best geometries obtained from the sensitivity analysis. The linear morphing methods (Tahara *et al.*, 2008) proved unsuitable for this purpose as the blister leading edge curvatures were smoothed out during the process. Hence, the particle swarms optimizer converged to one of the initial geometries used for the morphing optimization.

3.4. Re-evaluation of design variables

3.4.1. Blister design variables

A detailed analysis of the mechanism of action of the blisters was performed to obtain additional design variables for improved blister wave cancellation. Ten different designs were created with different leading edge vertical curvatures, and the solutions were analyzed. The slope of the leading edge was modified with both steps and smooth splines. The blister mid-body shape sensitivity study was also carried out to obtain the best shape for the viscous pressure recovery. The design modifications incorporate variations of tear-drop type streamlined shapes for the blister mid-body. Fifteen variations were designed and the solutions were analyzed. The best design further increased the resistance reduction, amounting to a total reduction of ~7% compared to base-line. The greatest resistance reduction was achieved when a vertical concave curvature was incorporated to the blister leading edge (Fig 8), such that the surface is normal to the incoming streamlines.

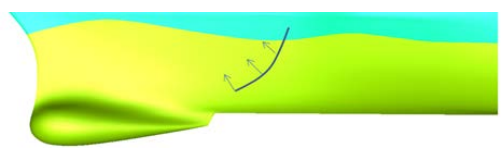

Fig. 8 Blister leading edge curvature

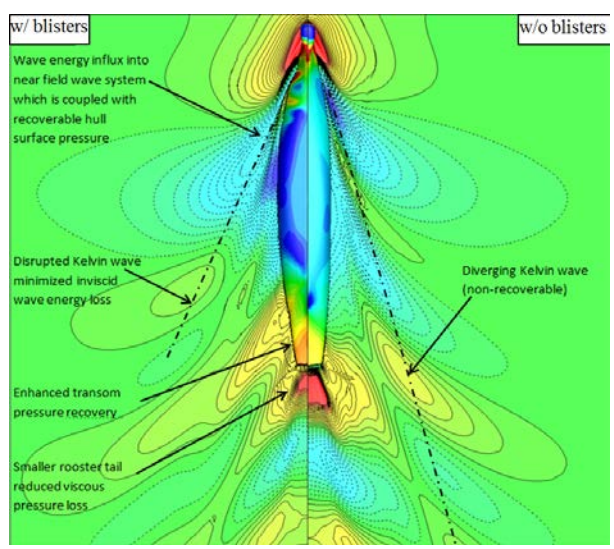

Fig. 9 Mechanism of blister action

The blister design reduces both the inviscid and viscous pressure losses as illustrated in Fig. 9. The in-viscid loss is the wave energy lost to the far-field Kelvin waves. The viscous loss is the energy lost to the transom wake in the form of a rooster tail. A portion of the wave energy that would normally be lost to the far-field Kelvin waves is transferred into the near-field wave system, and is recovered through transom pressure recovery. The blister mid-body optimization enhances the transom pressure recovery. The reduced rooster tail in the wake indicates the reduction in stern loss.

3.4.2. Design-variables modifications based on sea-keeping considerations

Previous studies have indicated that ships with natural roll-period less than 10 seconds are expected to encounter resonant waves significantly more often in the North Atlantic Ocean based on observed frequency of waves. Larger values for gyradius K_{XX} and smaller values for metacentric height GM increase the natural roll period, which varies linearly with K_{XX} and hyperbolically with GM. Though K_{XX} for the hybrid ships is larger due to the increased beam, the corresponding increase in water plane area moment of inertia counteracts its effects by increasing GM. Hence, the net effect of the blisters is a decrease in roll period from 11 to 8 seconds.

A new ship was designed with a shorter LWL, and larger draft to compensate for the displacement. A decrease in *Ixx* (moment of inertia of water-plane area about x axis) would lead to a decrease in CM = Ixx/volume, and hence a decrease in GM which would lead to larger hydrostatic roll period. The scaled design with LWL=140m (reduced from 143.56m) was the only design with roll period greater than 10s. To verify the hydrostatic roll period estimated using the formula, simulations were conducted with an initial roll angle of 20°, free to move with three degrees of freedom (3-DOF) for heave, pitch and roll. Peak to peak measurements indicate that the natural roll periods for the new design was 10.85s. Calm water resistance simulations at design speed 20 knots indicated a 6.5% full scale resistance reduction compared to variant 1 due to the same mechanism as previous designs, *i.e.*, enhanced pressure recovery due to the beneficial phase shift caused by the blisters. However, cost benefit analysis indicated that a change in LWL is unfeasible as it would affect outfitting and compartment drawings. The same applies to the bow and transom modifications, as they too affect outfitting and compartment drawings.

Table 2 provides a summary of the Phase I hybrid ship designs. The resistance characteristics of hulls with different displacement are compared using the non-dimensional transport factor (TF); larger values of TF indicate better transport efficiency.

Geometry	LWL (m)	Draft (m)	Beam (m)	KG (m)	KC (m)	I_{00} (m^4)	CM (m)	GM (m)	K_{XX} (m)	Mass - ρV (MT)	Resist. (KN)	Transp. fn. TF	Roll P. (s)	*Geometry particulars*
DDG-Variant 1	143.56	6.55	18.22	x	x	x	x	0.95	x	9590	x	x	14.5	***ONR (classified) Steel baseline***
5415-Variant 1 ***Δ % Var-1***	143.56	6.55	19.34	7.54	4.01	51548	5.51	1.98	7.05	9590 **0 %**	497 **0 %**	189 **0 %**	11.01 **0 %**	***UI Steel baseline***
5415 ***Δ % Var-1***	142.18	6.15	19.06	7.51	3.75	48187	5.72	1.96	7.62	8635 **↓ -10 %**	452 **↓ -9 %**	187 **↓ -1 %**	10.93 **↓ -7 %**	***5415 benchmark***
2B ***Δ % Var-1***	143.56	6.55	24.43	7.29	3.90	90989	7.47	4.08	8.30	12479 **30 %↑**	653 **31 %↑**	187 **↓ -1 %**	8.24 **↓ -25 %**	***2B - GRP bow, stern & blister/2C - GRP blister***
2B-mod. blister ***Δ % Var-1***	143.56	6.55	24.43	7.29	3.90	90548	7.44	4.05	8.30	12479 **30 %↑**	627 **26 %↑**	195 **3%↑**	8.28 **↓ -25 %**	***Opt. GRP blister***
3A ***Δ % Var-1***	143.56	6.55	18.22	7.62	4.03	46913	5.21	1.26	7.29	9237 **↓ -4 %**	496 **↓ -0.2 %**	183 **↓ -3%**	11.49 **4 %↑**	***Wave-piercing Steel baseline***
3B ***Δ % Var-1***	143.56	6.55	24.29	7.29	3.91	89236	7.67	4.28	8.26	11933 **24 %↑**	590 **18 %↑**	198 **5%↑**	8.00 **↓ -27 %**	***GRP bow, stern & blister***
Prelim-opt-3B ***Δ % Var-1***	143.56	6.55	22.14	7.55	3.95	66953	6.48	2.88	7.53	10590 **10 %↑**	500 **.5 %↑**	208 **10%↑**	8.89 **↓ -19 %**	***Opt. GRP bow, stern, blister***
Optimized-3B ***Δ % Var-1***	140.00	7.00	19.93	7.55	4.05	48236	4.90	1.40	6.73	10090 **5 %↑**	467 **↓ -6 %**	212 **12%↑**	11.39 **3 %↑**	***Opt. GRP bow, stern, blister, LWL***
3C ***Δ % Var-1***	143.56	6.55	24.29	7.29	3.91	89236	7.67	4.28	8.26	11933 **24 %↑**	590 **18 %↑**	198 **5%↑**	8.00 **↓ -27 %**	***GRP blister***
Optimized-3C ***Δ % Var-1***	143.56	5.70	25.88	7.55	3.25	92271	9.37	5.06	8.80	10090 **5 %↑**	458 **↓ -8 %**	216 **14%↑**	7.82 **↓ -29 %**	***Opt. GRP blister***

Table 2: Phase I hybrid ship designs

3.5. PHASE II studies

3.5.1. Introduction

Evaluation of the Phase I designs *w.r.t.* practicality of construction and operation indicated the following additional design criteria and constraints

1. Since the net effect of the blisters that cross the design waterline is a decrease in roll period, which is detrimental to operability in the North Atlantic Ocean, a paradigm change had to be implemented to the hybrid concept design.
2. The size of the blisters have to be reduced substantially, as the initial blister cost estimate was ~40M $ which is unfeasible.
3. Cost benefit analysis also dictated that the bow and transom

of the ship should be unaltered.

4. The draft of the ship needs to be unaltered
5. The blister design and optimization studies need to be conducted on DTMB-5415, instead of Phase I – design variant to facilitate code validation
6. The blister design needs to be integrated with a bow-bulb design
7. The blisters design optimization needs to be carried out for multiple speeds to reduce total annual cost of operation.

The performance of the blisters designs with blister weight of 3% and with 8% increased displacement to account for the 5% increase in payload has to be compared with the performance of the baseline 5415, which requires only 5% increase in displacement (albeit with increase draft, for the 5% increase in payload). The relevant ship variants to compare for the study are as follows:

1. Baseline 5415 (**5415**)
2. Baseline 5415 *w/* 5% increase in displacement (**54155%**)
3. 5415 w bow-bulb (**5415B**)
4. 5415 *w/* bow-bulb *w/* 5% increase in displacement (**5415B5%**)
5. 5415 *w/* blisters *w/* 8% increase in displacement (**5415BL8%**)
6. 5415 *w/* bow-bulb *w/* blisters *w/* 8% increase in displacement (**5415BLB8%**)

3.5.2. Grid design for baseline 5415

During Phase II, the initial grid design of 5415 was modified to account for the perceived locations of the new design variables for the blisters and the bow bulb, requiring a finer grid density at these locations. The grids and code were validated with data for 5415. Table 3 shows the grid and domain sizes for the grid study.

Table 3: Grids used for validation study

	Block name	Grid dimension (*imax*×*jmax*×*kmax*)	Grid pts	Total Grid points
Present work: 5415	Ship hull	177×107×154	2,916,606	**7,8**26,979 (7.8M)
	Transom stern	30×107×96	308,160	
	Background	229×77×261	4,602,213	
Present work: 5415M	Ship hull	173×44×83	631,796	**8,1**43,350 (8.1M)
	Near-field refinement	201×51×151	1,547,901	
	Wake refinement	134×40×254	1,361,440	
	Background	229×77×261	4,602,213	
Present work: 5415b	Ship hull	177×107×154	2,916,606	**10,**736,320 (10.7M)
	Transom stern	30×107×96	308,160	
	Near-field refinement	201×51×151	1,547,901	
	Wake refinement	134×40×254	1,361,440	
	Background	229×77×261	4,602,213	
Carrica et al. (2007):5415(Fine*) Sea-keeping and calm water Free to heave and pitch	Ship hull	173×51×83	732,309	**2,9**63,923 (3M)
	Refinement	217×57×121	1,496,649	
	Background	161×55×83	734,965	
Xing et al. (2009) Calm water Free to heave and pitch	Ship hull	122×36×58	254,736	**1,2**90672 (1.3M)
	Refinement	153×40×85	520,200	
	Background	114×78×58	515,736	
Xing et al. (2009) Fixed zero sinkage and trim	Single block	142×61×71	615,002	0.6M

3.5.3. Grid and code validation for baseline 5415

The calm water validation was performed using data from Longo and Stern, (2005), and the errors are compared with validation errors from Gothenburg 2010 test cases. The average validation error for C_T in the current case is smaller than previous validation studies when refinement blocks are used in the near field region. Without near-field refinement, the errors are of similar magnitude as the other validation studies.

Fig. 10 shows the validation results of the resistance, sinkage and trim over the Fr range. The average resistance error over the Fr range is 4.7% and 0.52%, for grids *w/o* and *w/* near-field refinement, respectively. The average error of the Gothenburg 2010 validation cases from all the different codes was 3.16%. The average sinkage error over the Fr range is 15.77% and 17.01%, for grids *w/o* and *w/* near-field refinement, respectively.

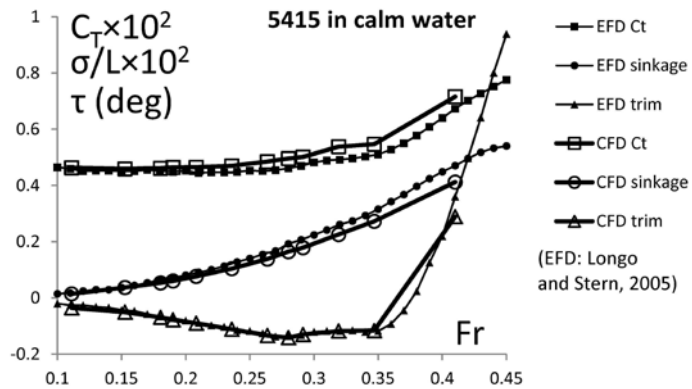

Fig. 10 Total resistance coefficient, sinkage and trim for 5415 hull in calm water

The average error of the Gothenburg 2010 validation cases from all the different codes was 16.8%. The average trim error over the Fr range is 5.58% and 23.95%, for grids *w/o* and *w/* near-field refinement, respectively. The average error of the Gothenburg 2010 validation cases from all the different codes was 69.23%. Sinkage and trim calculations normally have a higher error than the resistance calculations since their values are much smaller and they are a second order hydrodynamic effect.

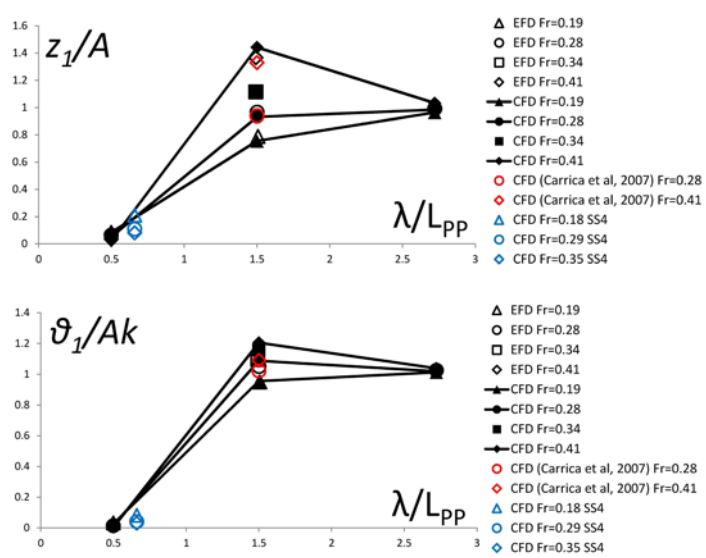

Fig. 11 Heave and pitch amplitude of 5415 hull for validation

The sea-keeping validation (Fig. 11) was performed using data from Irvine *et al.* (2008), and compared with previous validation results from Carrica *et al.* (2007). The validation data include pitch and heave responses; resistance data was unavailable. The averages errors for heave and pitch are 10.64% and 59.4%, respectively. Again, the error values are high because of its proximity to zero.

3.5.4. Paradigm change in design for Phase II

To address the sea-keeping problem, the blisters were modified to be entirely submerged, while keeping most of the wave-cancellation design features intact, so that the water-plane area does not increase (Fig. 12). The submerged blisters also substantially reduce the surface area and associated cost compared to the Phase I blisters.

Initial submerged blister designs were generated by replicating the design features of the Phase I optimized ship as best as possible, while subject to the new geometry criteria.

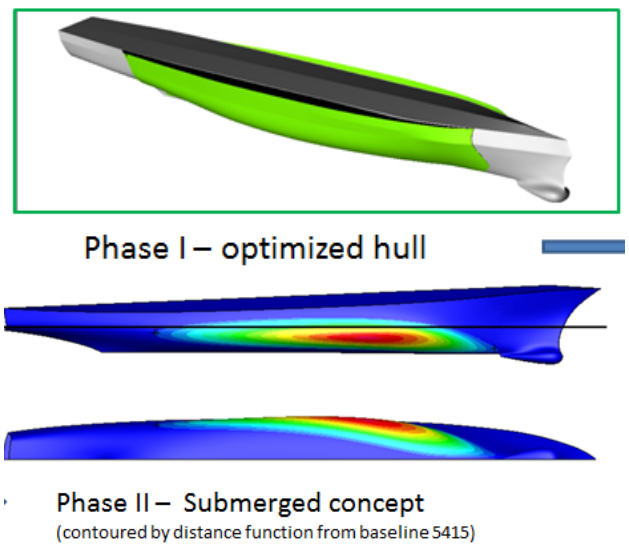

Fig. 12 Paradigm change after concept evaluation

Roll-period calculations (Table 4) of the new concepts indicated that the values fall in the desired range, similar to the baseline 5415 design.

Table 4: Mass property and hydrostatic estimates for roll period

Geometry	*Mass (MT)*	*Vol. (m^3)*	*Draft (m)*	*Beam (m)*	*Aw (m^2)*	*Ixx (m^4)*	*CM (m)*
5415	8633	8422	6.15	19.06	2097	49204	5.84
5415B	8647	8436	6.15	19.06	2098	49202	5.83
54155%	9036	8816	6.37	19.11	2115	50148	5.69
5415B5%	9026	8806	6.36	19.11	2114	50082	5.69
5415BL8%	9297	9070	6.18	19.66	2132	52139	5.75
5415BLB8%	9299	9072	6.17	19.67	2133	52149	5.75

Aw = Water-plane area
Ixx = Moment of inertia of water-plane area (*Aw*) about x axis
CM = Metacentric height from center of buoyancy = *Ixx*/Volume

Geometry	*KC (m)*	*KM (m)*	*KG (m)*	*GM (m)*	*Kxx =0.4B (m)*	*Roll P. (s)*
5415	3.66	9.50	7.57	1.93	7.62	11.00
5415B	3.66	9.49	7.57	1.92	7.62	11.03
54155%	3.81	9.50	7.79	1.71	7.64	11.73
5415B5%	3.80	9.49	7.78	1.71	7.64	11.74
5415BL8%	3.72	9.47	7.60	1.87	7.86	11.54
5415BLB8%	3.71	9.46	7.59	1.87	7.87	11.55

KC = Center of buoyancy measured from keel
KM = Metacentric height measured from keel = KC+CM
KG = Vertical center of gravity measured from keel
GM = Stability index = KM-KG
Kxx = Roll radius of gyration = 0.4×Beam
Roll P. = Hydrostatic roll period = $2\pi K_{XX}/\sqrt{g \times GM}$

3.5.5. Formulation of design variables

<u>3.5.5.1. Initial formulation of blister design variables for single speed resistance</u>

Solutions from the initial blister design showed negligible improvement in TF, because of the additional constraints. The CFD solutions were analyzed to find correlations between the blister topology and cancelation effect on the shoulder wave. Based on these correlations, new blister topologies were produced by using a combination of involutes, sigmoid, tear-drop, and Gompertz functions.

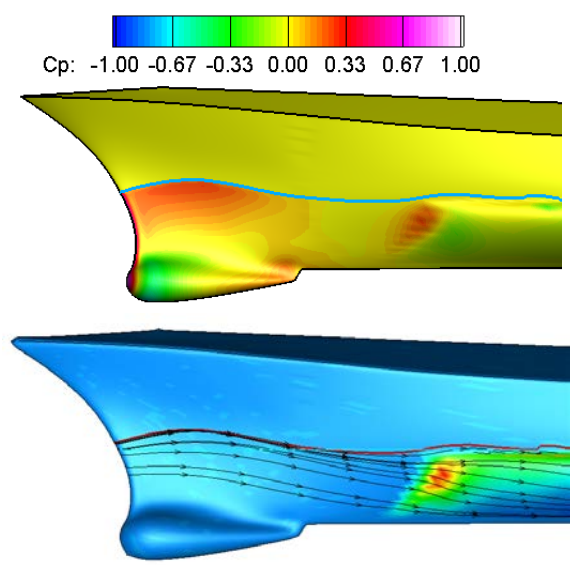

Fig. 13 Blister leading edge design in x-z plane: (a) hull surface pressure contours; (b) blister steepness

Multiple submerged blister designs were created, and the CFD solutions analyzed to find correlations between the blister leading edge location, longitudinal slope and normal steepness *w.r.t.* the leading diverging wavelength and angle of divergence which are mainly dependent on the Fr and the ship slenderness ratio. The phase wave front is formed by the bow geometry and forms a group of far-field waves and Kelvin angle $\alpha \leq 19^{o}$ given

by dispersion relations. Phase cancellation of the phase wave front of the bow wave minimizes the energy lost in the Kelvin wave packet front. For DTMB-5415 at Fr=0.28, $\lambda/L = 2\pi Fr^2 = 0.5$. Hence, the blister leading edge should be located at x/L=0.25, and the mean angle of the blister leading edge based on the propagation velocity of the phase wave front should be $\theta \sim 55^o$. The blister steepness function dictates the location of maximum hull surface pressure, which in turn produces the wave-cancellation effect. The maximum steepness should occur at the plane whose tangent vectors are normal to the mid-point tangent vectors of the descending bow wave. Fig. 13 shows the correlation between blister steepness and pressure.

Through progressive flow analysis of effects of geometry variations, geometries was produced with best slope and steepness functions for shoulder wave cancellation and destructive interference of the diverging Kelvin wave. The geometry was further modified for better natural roll period characteristics, and blister size reduction for production cost feasibility, which was the secondary objective. The blister volume was constrained to displace exactly 8% of the original displacement so that there is no change in the static draft. This was done to ensure no major modifications to the propulsion systems, deck height and any other related structural factors.

3.5.5.2. Multi-speed blister design formulation

Designing blisters for a specific speed (20 knots) results in penalties at off-design speeds. The next stage of the design progression expanded the design envelope from single-speed to multi-speed using incremental blister concepts which enabled wave-cancellation over a speed range. Fig. 14 provides the total annual costs for the different speeds of operation using a weighted distribution of the 76,269 bbls/yr at $175/bbl over the speed-time profiles (Naval sea systems command, 2012) based on the effective power calculations at each speed for DTMB 5415.

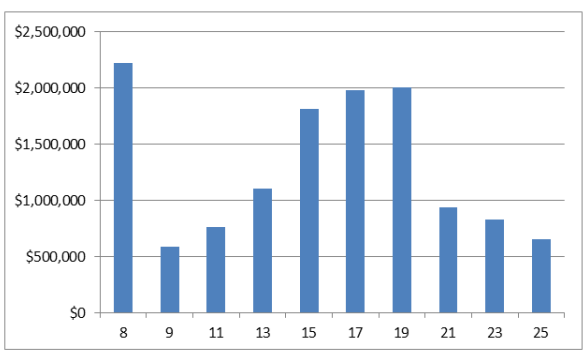

Fig. 14 Annual fuel cost

3.5.5.3. Multi-speed design variables

Since most of the operational costs falls at 15-19 knots range, the blister concept is designed for this range. Note that frictional resistance plays a larger role for Fr=0.19 compared to Fr=0.28 and there are two smaller waves in the fore-ship section for Fr=0.19 compared to one bigger wave for Fr=0.28.

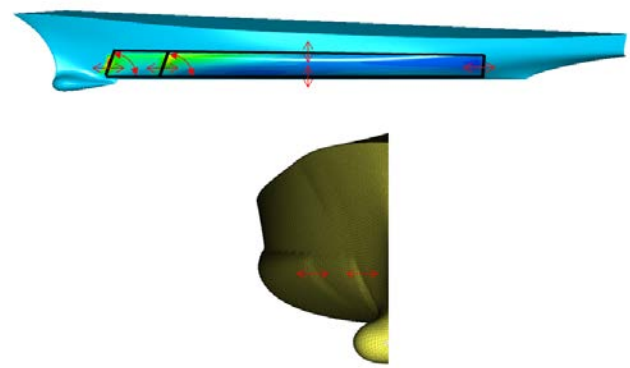

Fig. 15 Design variables for multi-speed optimization: 5 translations, 2 rotations, 2 expansions

An incremental blister concept (Fig. 15) was designed to preserve the wave-cancellation properties over this speed range. The preceding retrofitted blister which was designed specifically for design speed of 20 knots was advanced for performance improvement over the design speed range 15-19 knots, which accounts for ~50% of in-transit fuel. The new geometry incorporates incremental blister design and shows resistance improvement over the speed range 15-19 knots.

3.5.5.4. Structural constraints

Structural analysis, which will be discussed in detail in forthcoming sections, dictated that the blister edges need to be located at deck locations on the ship, failing which they would be a '*can-opener effect*' due to the bending moments. Hence the design variables were modified with a sigma function at the top edge to fillet the blister into the deck location (Fig 16).

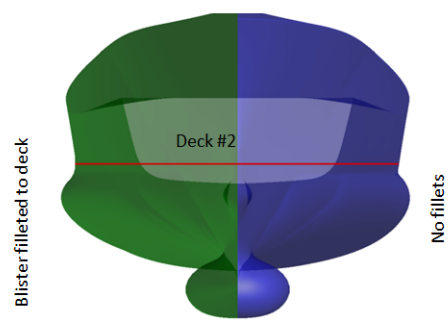

Fig. 16 Blister filleted to the deck

3.5.5.5. Blister cost function

Reduction of the blister cost function is the secondary objective for the optimization. The blister cost is estimated using simple formulae based on its surface area, i.e., cost = surface area × weight/area × cost/weight, which contracts to cost = 375 × surface area. Being a secondary objective function, designs with lower blister costs were pursued only if they had no negative impact on the resistance characteristics which directly affect life cycle costs.

3.5.5.6. Bow-bulb concepts

The initial 5415 bow bulb design was created using the non-dimensional design parameters on the size and location obtained from Cusanelli (1998). CFD calculations indicated ~2% resistance reduction at 20 knots, i.e., a PE ratio of 0.98 compared to 0.912 for DDG-51. The bow bulb was then modified using a systematic sensitivity analysis of the size, aspect ratios and distance from the waterline for best resistance reduction at three speeds 15, 17 and 19 knots.

Fig. 17 Bow bulb design – tear drop *vs.* prolate spheroid

A better reduction was possible by converting the tear drop bulb profile into a prolate spheroid with its leading edge slope matching the leading edge slope of the hull for phase velocity equivalence of the two cancelling wave groups (Fig 17). The sharper leading edge also reduces the viscous loss caused by the blunt tear-drop. The bulb was then incorporated along with the blister design which showed reduction of both the bow and the shoulder waves.

3.5.5.7. Combined blister and bow-bulb concepts

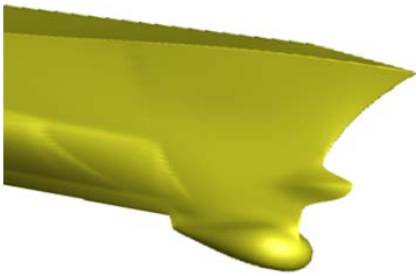

Fig. 18 Combined blister and bow-bulb design

The best bow bulb was then incorporated into the blistered ship design (Fig 18). The bow bulb design variables were tuned to account for the flow modification induced by the blister and optimized further. Seventy different designs simulations were performed within the upper and lower bounds of the nine design variables.

3.5.6. Quantitative analysis of the results

3.5.6.1 Calm water analysis

Calm water resistance results were obtained over the entire Fr range. Note that 54155% and 5415B5% geometries have larger drafts compared to the original to accommodate the 5% increase in displacement, whereas 5415BL8% and 5415BLB8% have the same draft as the original, with the 8% larger displacement accounted for by the blister volume.

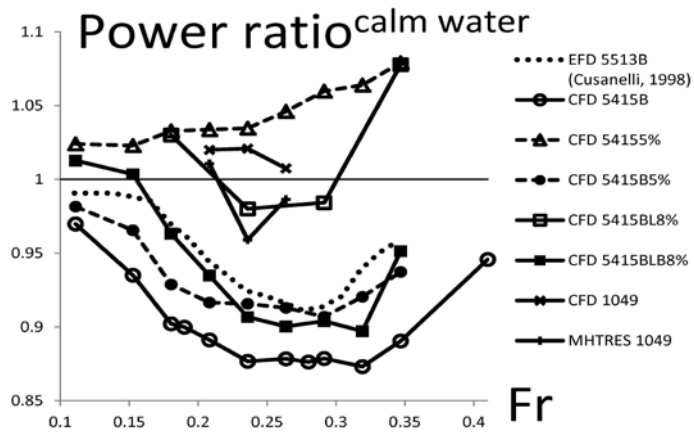

Fig. 19 Power ratios *w.r.t.* baseline 5415 over operational speed range

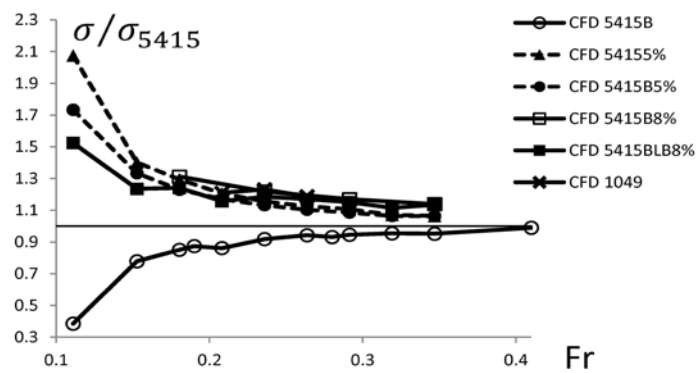

Fig. 20 Sinkage ratios *w.r.t.* baseline 5415 over operational speed range

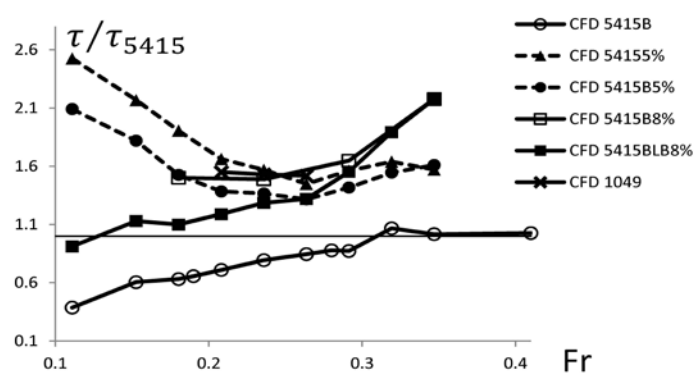

Fig. 21 Trim ratios *w.r.t.* baseline 5415 over operational speed range

Fig. 19 provides a comparison of the powering performance of the different variants *w.r.t* the baseline 5415, along with the

EFD data from Cusanelli (1998), for model 5513 with bow-bulb using power ratios. Also included in the figure are the URANS solutions of the 1049 geometry, the optimal solution produced by the multi-criterion hydrodynamic analysis using the MHTRES thin-ship theory code. Contrary to the MHTRES solutions, the URANS solutions do not indicate a powering reduction for the 1049 geometry. Figs. 20 and 21 show the sinkage and trim ratios, respectively.

5415B

The new bow-bulb design shows a resistance reduction of ~12% over the Fr range. The bow-bulb, which is modeled after a prolate spheroid performs better than the tear-drop shaped bow bulb from Cusanelli (1998), which shows a resistance reduction ranging from 3 to 9% in the Fr range. The bow bulb has an effect of reducing both the sinkage and trim over the Fr range, with values tending towards baseline with increase in Fr.

5415B5%

Increasing the displacement of the bow-bulb 5415 by 5% still gives a reduction of 7-8% over the Fr range compared to the baseline 5415. However, compared to the 54155%, *i.e.*, baseline 5415 with 5% greater displacement, the resistance reduction is around 12-14% over the Fr range. Though the bow-bulb reduces the sinkage and trim in the baseline draft configuration, an increase in displacement reverses the trend with increased sinkage and trim over the Fr range, with values tending towards baseline with increase in Fr.

5415BL8%

The blisters were optimized for speeds 15 to 19 knots, which correspond to Fr range of 0.22 to 0.27. At this range the blistered ship indicated a resistance reduction of ~2% compared to the baseline, in spite of the 8% larger displacement. The more relevant comparison is with 54155%, which shows a reduction of 4 to 8% over the design Fr range. The blister cost was estimated to be $5.65M. Similar to 5415B5%, results indicate increased sinkage and trim over the Fr range, with sinkage values tending towards baseline with increase in Fr.

5415BLB8%

The final combined blister and bulb design indicates a resistance reduction of 6 to 12% compared to the baseline 5415 and a reduction of 7 to 20% compared to 54155%. Similar to 5415B5%, results indicate increased sinkage and trim over the Fr range, with sinkage values tending towards baseline with increase in Fr. Figures 22, 23, and 24 show the reduction of the bow and the shoulder waves due to the combined action of the bow-bulb and blisters at 19, 17 and 15 knots.

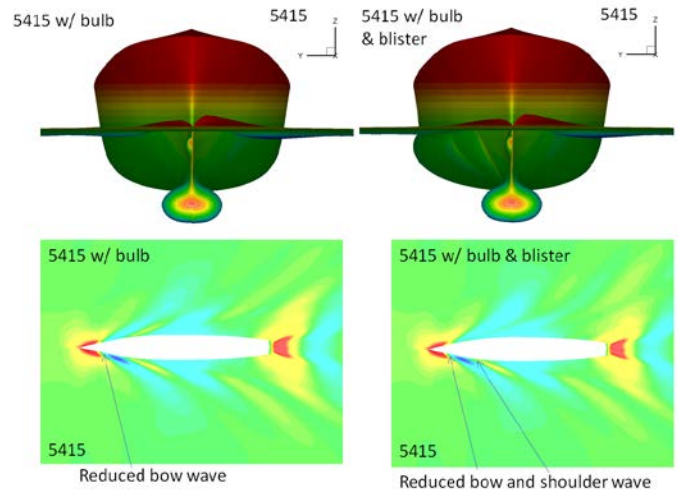

Fig. 22 Combined bow bulb and blister effects at 19 knots

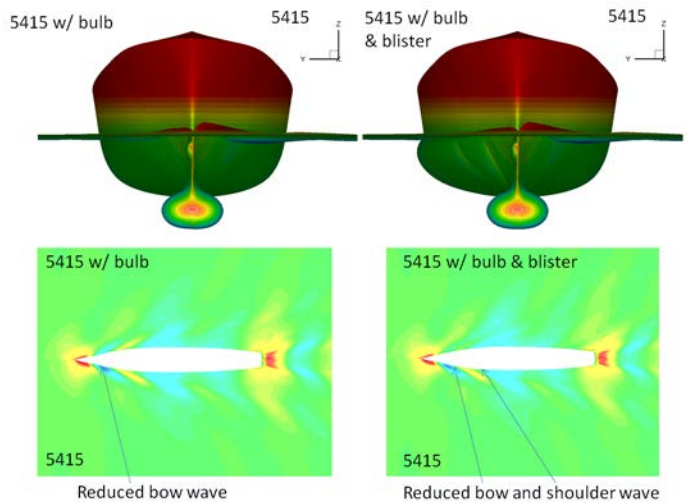

Fig. 23 Combined bow bulb and blister effects at 17 knots

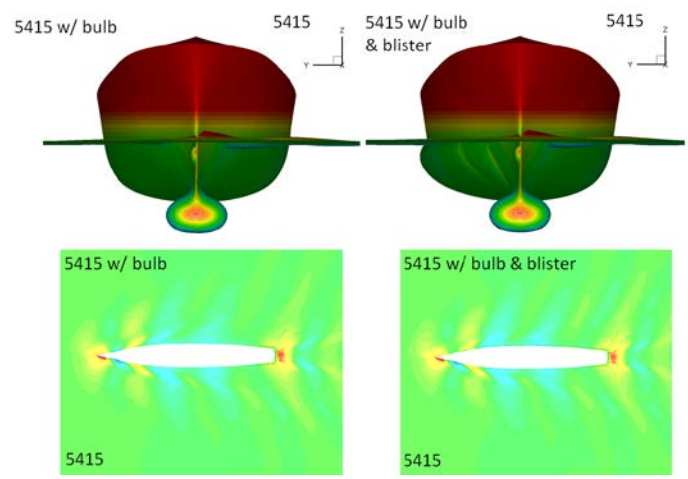

Fig. 24 Combined bow bulb and blister effects at 15 knots

3.5.6.2. Sea-keeping analysis

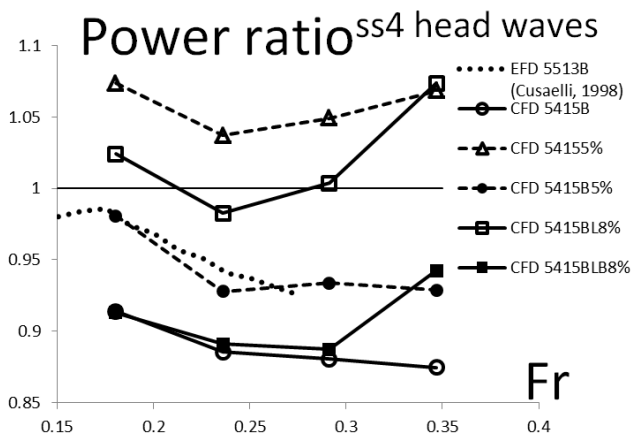

Fig. 25 Performance comparison over operational speed range in SS4 head waves

The power ratio was also calculated in the most probable sea-state (SS4) in both head (Fig 25) and following waves (Fig 26). The overall trend is similar to the calm water calculations.

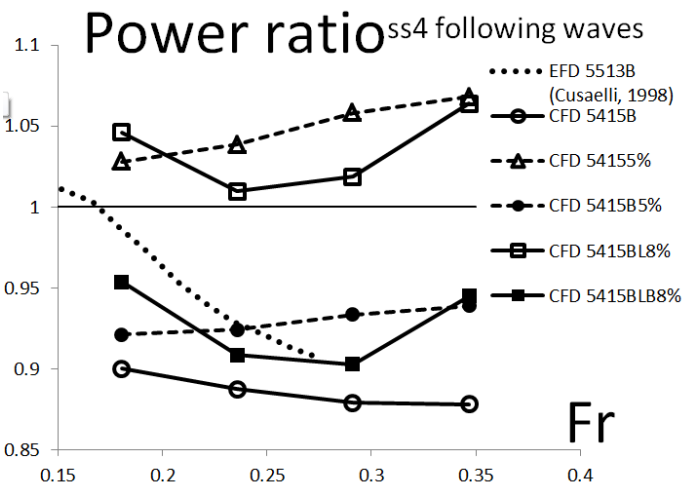

Fig. 26 Performance comparison over operational speed range in SS4 following waves

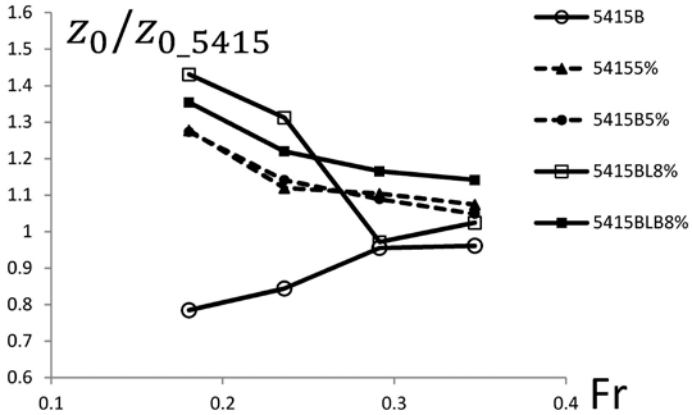

Fig. 27 Heave mean values in SS4 head waves

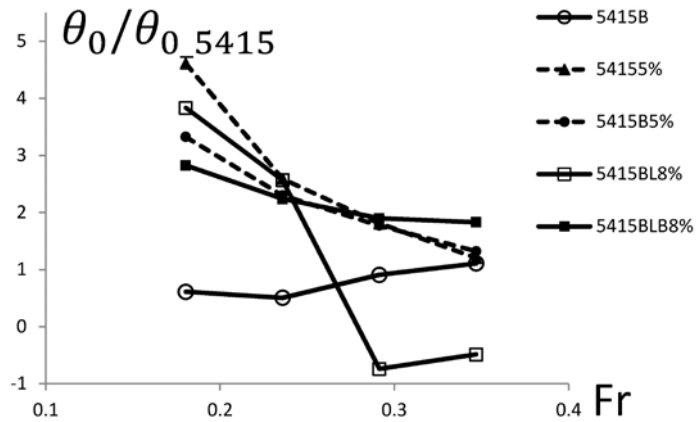

Fig. 28 Pitch mean values in SS4 head waves

The average heave and pitch calculations in SS4 head waves show similar trend as the sinkage and trim calculations over the Fr range (Figs 27, 28). i.e., the bow bulb by itself has an effect of reducing both the sinkage and trim over the Fr range, with values tending towards baseline with increase in Fr. Though the bow-bulb reduces the mean heave and pitch in the baseline draft configuration, an increase in displacement reverses the trend with increased sinkage and trim over the Fr range, with values tending towards baseline with increase in Fr. There is a sudden drop in both mean heave and pitch values at Fr~0.25 for 5415BL8% design.

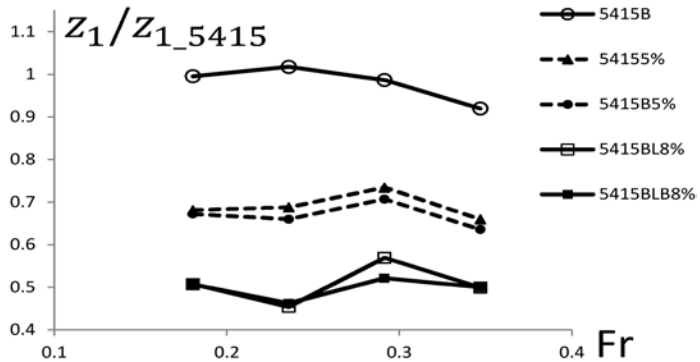

Fig. 29 Heave amplitude ratio of different configurations to original 5415 hull in different Fr and sea state 4 head waves

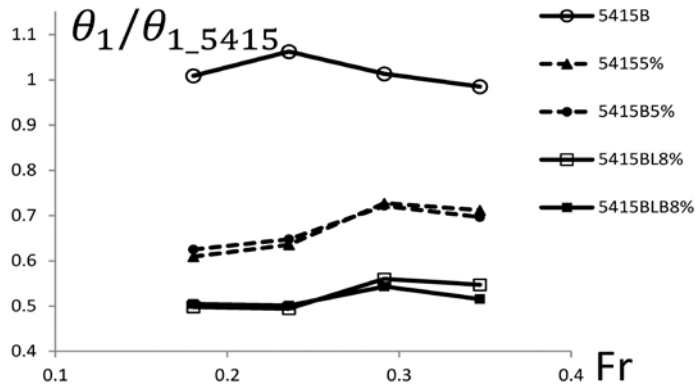

Fig. 30 Pitch amplitude ratio of different configurations to original 5415 hull in different Fr and sea state 4 head waves

The blisters damp out the motions and the heave (Fig 29) and pitch (Fig 30) amplitudes of the variants with the blisters are half as that of the baseline 5415. Also, increasing the draft of the ship reduces the heave and pitch amplitude as seen from the results for 54155% and 5415B5% variants. This damping effect on the motions due to the blisters also reduces the added resistance for the variants with the blisters compared to the baseline 5415 (Fig. 31).

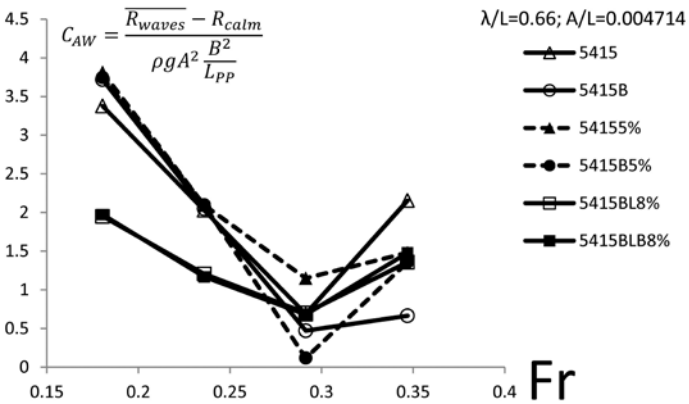

Fig. 31 Added resistance coefficient in different Fr and sea state 4 head waves

3.6. Annual cost of operation

The annual fuel cost calculation method follows Cusanelli and Karafiath (2012). Full-scale power (SHP) is entered for each speed in the profile. At each speed in the profile, underway propulsion fuel consumption rates are produced by interpolation along the measured curves of underway propulsion engine fuel rates *vs.* SHP. The interpolated engine fuel rates are then multiplied by the resultant number of hours/year for each speed in the profile, producing values of barrels/year at each speed in the profile. Annual underway propulsion fuel consumption is the summation of the fuel consumptions at all the speeds in the profile, expressed as total barrels/year. *Hydrodynamic power = hydrodynamic resistance × velocity.* This was multiplied by the estimated propeller delivered efficiency (Cusanelli and Karafiath, 2012) to get the shaft power. These findings are summarized as follows:

At $175/barrel, the annual fuel cost for DTMB 5415 is $5.65M
A 5% increase in payload increases the cost by $156, 940 (+2.8%)
A 5% increase in payload along with the new bow bulb design reduces the cost by $194,424 (-3.4%)
A 5% increase in payload with both bow bulb and blister reduces the cost by $171,240 (-3.0%)

4. MULTICRITERION HYDRODYNAMIC ANALYSIS

4.1 Problem Formulation

For practical and academic reasons, there was a desire to explore this design problem using fast physics-based, lower-order analysis and design tools. From a practical perspective it is desirable to solve this design problem resulting in solution(s) with: improved hydrodynamic performance; minimal analysis time per solution to allow more design options to be subsequently investigated. From an academic perspective it is desirable to understand how these tools integrate in dynamic problem solving, and how the approach may be extended and improved. The following discussion will focus on the practical aspects of the problem.

The problem of finding solutions to a ship design requiring increased displacement with minimal impact to seakeeping and powering performance, and minimal cost of applying the hull blister was formulated as an evolutionary, multicriterion design optimization problem (Zalek et al, 2009). The optimization problem was formulated with the three previously mentioned goals, or objective-functions, as numerical measures of merit: a composite value for minimal hull resistance across a range of speeds; a composite value for maximum seakeeping performance across a range of conditions and performance criteria; and minimal estimated cost of applying the hull blister which was related to its geometry. The design constraints included adding 800 metric tons of hull displacement and the blister geometry being anchored along its length to positions corresponding to interior decks for support. In order to help improve the powering performance, a bow bulb was also added to the design.

The design optimization algorithm is an automated process with heuristics to generate and analyze solutions in a relatively efficient manner, ultimately providing a set of feasible, non-dominated design trade-off solutions with respect to the three goals. Its formulation is described in Zalek et al (2009). Certain optimization control parameters dictate how many solutions are generated and analyzed, how deterministic and stochastic processes are applied to generating new solutions, and how long the overall process runs. These parameters have been tested and set to achieve robust, repeatable results for this problem.

The baseline hull form was the DTMB-5415 design. The hull geometry was modified according to a set of analytic functions over a designed domain on the hull form. Both the blister and bow bulb were described using these equations, and each used their own unique set of shape parameters. Using analytic functions to implement hull form shape variation is one way to ensure a fair hull form where desired. The hydrodynamic analysis tools utilize a hull offset file (set of {x, y, z} coordinates) to describe the hull form geometry. The analytic functions were applied to a designated region (Δx × Δz) of the hull form offset file in a manner that extended the girth in the transverse (y-axis) direction only, as shown in the following equations:

$$y_x(x_i) = \left[\sin\left(\pi \cdot \left(\frac{x_i}{\Delta x}\right)^{n_{1x}}\right)\right]^{n_{2x}}$$
$$y_z(z_{ij}) = \left[\sin\left(\pi \cdot \left(\frac{z_{ij}}{\Delta z}\right)^{n_{1z}}\right)\right]^{n_{2z}}$$

$$y_{xz}(x_i, z_{ij}) = y_x \cdot y_z$$

Both equations y_x and y_z each have two shape parameters, n_1 and n_2, and a single directional flag, for a total of six shape alteration variables. Examples of the hull form shape functions are shown in Figure 32. The hull form modification region bounds are also variables; two bounds each for Δx (fore and aft) and Δz (upper and lower) for a total of four additional variables. The shape functions in the x-direction and z-direction are combined in the function y_{xz}.

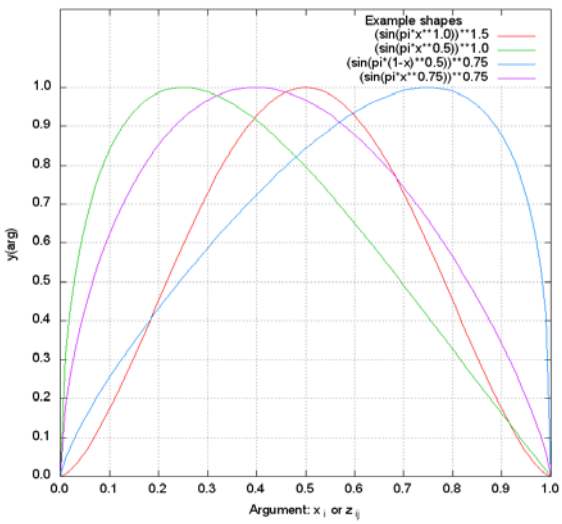

Fig. 32 Examples of hull form blister shape functions

The blister cost was estimated to be related to the amount of material (steel) required for its construction: 15 pounds of steel per square foot of blister surface area × $25 per pound of steel = $375 per square foot of blister surface area added to the hull.

Hull seakeeping analysis was conducted with the SHIPMO.BM (Beck and Troesch, 1989) linear strip-theory seakeeping program. The SIPMO.BM linear seakeeping analysis program (Beck and Troesch, 1989) predicts ship motions in six degrees of freedom and five components of shear and bending moment distributions. It is based upon the strip theory approach of Salvensen et al. (1970) with the method extended by Beck et al. (1989) to include the surge motion analysis. The program has the capability to include a single symmetric pair of hull appendages mirrored across the centerline of the hull, such as static bilge keels.

The SHIPMO.BM program input requires a hull form offset file, weight distribution, seas characteristics (e.g. sea spectrum $S(\omega)$ and frequency range), ship speed(s), and heading angles relative to the seas, β. It can also take a list of P_M coordinates on the ship $\{x, y, z\}_m$, the locations of motions of interest. The SHIPMO.BM program returns the ship motion response (magnitude, velocity and/or acceleration) and phase shift for the given wave frequency domain for the six degrees of freedom and the ship motion points $\{x, y, z\}_m$. This analysis is performed for every combination of seas characteristics, ship speed and relative heading angle.

The measure of seakeeping performance was defined by a performance index (*SPI*) as described by Keane and Sandberg (1984) and has a value between 0 and 1.0. It considers the seakeeping performance of the ship with regard to its environment, operating condition and its operational goals. A ship that can achieve more of its operational goals in a given environment receives a higher seakeeping performance index.

The seakeeping performance index is discretized with respect to the probabilities assigned to: ship heading angle β relative to the seas; ship speed, V; sea state $S(\omega)$; and a set of operational ship motion limits σ^{limit}, at prescribed locations. A ship motion σ at a prescribed location m for the ith hull solution $\tilde{x}^i$ makes a positive contribution to the performance index in the amount of $P(\beta_j, V_k, S(\omega)_k, \{\sigma^{limit}\}_m)$. The *SPI* is defined as:

$$SPI(\tilde{x}^i) = \sum_{jklm} \left(f\left(\{\sigma_{jkl}(\tilde{x}^i)\}_m \leq \{\sigma^{limit}\}_m \right) \rightarrow [0 \; or \; 1] \right) \times P(\beta_j, V_k, S(\omega)_k, \{\sigma^{limit}\}_m)$$

The probability assigned to the encountered heading angle, $P(\beta)$ is evenly distributed among the angles of 0 degrees to 180 degrees in 15 degree increments.

The speed profile used as input to the seakeeping analysis was derived from recent studies of DDG-51 class ships operational records (Anderson et al, 2013). The speed profile used is shown in Table 5.

Table 5: Speed profile (in knots) and percentage of the time, *P*, the ship is expected to operate at that speed

V	0	5	10	15	20	25	knots
P	0.03	0.36	0.20	0.20	0.14	0.07	∑=1

The ship is expected to operate in a variety of environmental conditions. The sea conditions and probability of encounter are derived from tabulated environmental conditions of the open ocean in the north Atlantic from Principles of Naval Architecture, Vol. III (Lewis, 1989). Table 6 identifies the sea state parameters (significant wave height, H_S, and characteristic period, T_1) used to generate the JONSWAP sea spectrum $S(\omega)$ as input to the seakeeping analysis.

Table 6: Seas state (SS) conditions and probability of occurrence *P*

SS	**2**	**3**	**4**	**5**	**6**	**7**	
HS	0.30	0.88	1.88	3.25	5.00	7.50	m
T1	7.5	7.5	8.8	9.70	12.4	15.0	sec
P	0.08	0.24	0.28	0.21	0.13	0.06	∑=1

The motion limits for given operational activities are shown in Table 7. The two operational activities are transiting, and conducting helicopter operations. The limits used are based on human factors and other considerations.

The *SPI* requires the calculation of 13 relative heading angles ×

6 speeds × 6 sea states × 7 unique motion points = 3,276 motion response values per solution evaluated. The SHIPMO.BM seakeeping code was modified to perform these computations with a single function call. Given these parameters, the baseline DTMB-5415 hull form (without the DDG-51 type bilge keels) has a *SPI* of 0.61296. The *SPI* formulation is multimodal and its values are discreet. It is possible for two dissimilar ships to have the same SPI value, yet have a different distribution of performance cases that are satisfied.

Table 7: Motion limits for prescribed operational activities

Transit	**P**	**0.70**	**Limit**
Pitch			2.0 deg RMS
Roll			1.5 deg RMS
Deck house	Lateral	Accel.	0.1 g RMS
Deck house	Vertical	Accel.	0.2 g RMS

a) Transiting operations acceptable motion limits

Helicopter	**P**	**0.30**	**Limit**
Pitch			2.0 deg RMS
Roll			0.75 deg RMS
Helo deck	Lateral	Accel.	0.1 g RMS
Helo deck	Vertical	Accel.	0.2 g RMS
Helo deck	Vertical	Velocity	1.0 m/s RMS

b) Helicopter operations acceptable motion limits

The hull calm water resistance analysis was conducted with the MHTRES program developed by Larry Doctors to predict the components of resistance for monohull, multihull, surface-effect-ship and air cushion vehicle type vessels. The wave-resistance theory is the same as that pioneered by Michell (1898). In this theory, the ship is assumed to be thin and it is modeled mathematically as a source distribution on the submerged center-plane. Many experimental projects conducted in the last few decades have verified that this theory provides a good engineering prediction of the wave resistance for most monohull vessels. The current practical numerical implementation of the theory is based on representing the hull function (the local beam of the hull) as a series of overlapping tent functions; the height of the tent is equivalent to the local beam, while its base covers a small rectangular patch on the centerplane. The advantage of this technique is that the required wave functions can be integrated analytically. This leads to a compact and fast-running computer program, in which the number of tent functions can be as low as 60 longitudinally and 20 vertically. The formulas for the tent functions were published by Doctors (2012).

The representative resistance of the hull was taken to be the average of three total resistance values at three different speeds (15, 17, 19 knots), normalized by the baseline hull resistance values at those speeds. This composite resistance score places equal weight on the performance value at each of these speeds. A different set of speeds with a different weighting structure could result in different design solutions being considered as better design trade-off solutions.

4.2 Solution Results

The optimization process was run for 30 iterations, generating and evaluating a total of 3250 design solutions. This required approximately 12 hours of run-time on an Intel Core i7-3770 8-core CPU at 3.4 GHz and 16GB RAM running the Debian Linux operating system, with the 3.14.15_x64 GNU/Linux kernel. The optimization duration could be reduced through basic parallel processing during the solution hydrodynamic analysis phase. Performance tests indicate that the optimization solution set converges well for this set of parameters. The final design trade-off solution set (Pareto front) of 284 solutions is shown in Figures 33 and 34.

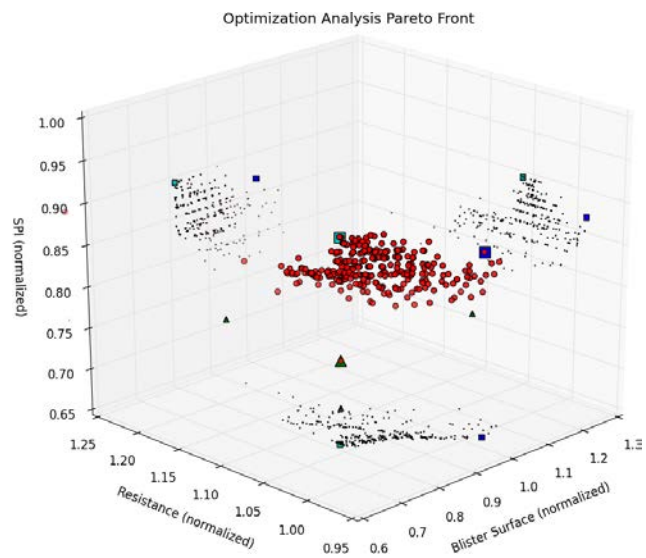

Fig. 33 Optimization analysis Pareto front in normalized form

The red circles plotted in Figure 33 show the solutions in non-dimensional objective-function space. It can be difficult to get a complete view of the plotted solutions in three-dimensional space using a static image, so the solutions have also been plotted on to the back and lower bounding planes in small dots. The axes have been arranged such that the solution region low and closest to the viewer is preferable.

The three objective functions were normalized in order to have the optimization process operate with objective function values of roughly the same scale, which can help mitigate potential scale-related issues. The blister area was normalized by a 'midpoint' surface area value (shape variables placed at the midpoint of the allowable range) which still generated 800 mt of additional required volume. The *SPI* measure was normalized by the baseline DTMB-5415 value (no blister), and it is also reformulated to be a measure of non-performance (1.0 - *SPI*). This means that the optimization process was attempting to minimize seakeeping non-performance. The hull resistance values were normalized by the baseline DTMB-5415 hull resistance values. The better solutions have minimal values in each category.

Useful qualitative information can be derived from the normalized results. For instance, all of the solutions have a normalized *SPI* value of less than unity. This means that the seakeeping non-performance of these solutions is less than that of the baseline design; all of these solutions have a better overall seakeeping performance than the baseline design. Some solutions do have a normalized resistance measure of merit of less than 1.0, but not many. These solutions are worth investigating more closely as the operating costs for these designs could be lower than the baseline design due to reduced fuel consumption.

A few solutions of interest have been marked with special symbols, both in space and projected on to the boundary planes. The nearest-to-utopian solution is marked with a green triangle. This is the solution nearest (L2-norm) to the ideal, or utopian, solution defined with the best (lowest) objective-function values from the solution set combined into a single solution. In this case it is interesting from an academic point of view, but it has a relatively high resistance and blister surface size compared to other solutions. The solution with the lowest resistance objective-function value is marked with a dark blue square; this is solution number 2850. The solution with the lowest blister objective-function value is marked with a light-blue square; this is solution number 1049. These solutions will be discussed further.

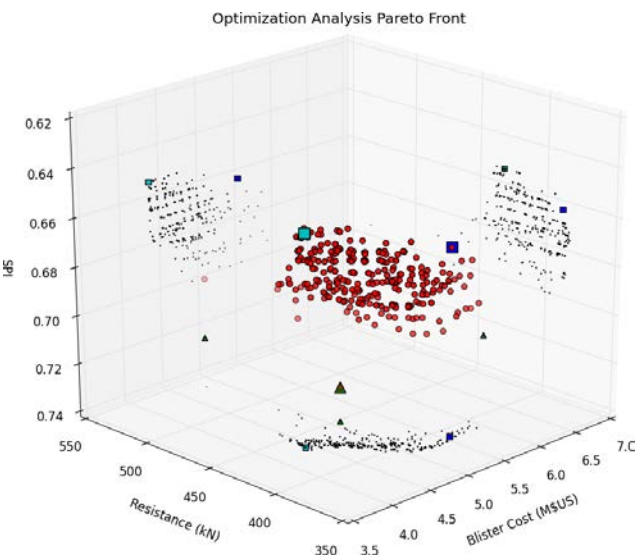

Fig. 34 Optimization analysis Pareto front in dimensional form.

Figure 34 shows the same optimization Pareto front solution set in dimensional form, and is marked in a manner similar to Figure 33. The blister cost is presented in $US, hull resistance in newtons and the seakeeping performance in the original *SPI* formulation. Hence, better solutions will have lower cost, reduced resistance and a higher SPI value. The axes have been arranged such that the solution region low and closest to the viewer is preferable. Resistance was calculated at three different speeds for each solution, but only the resistance from the top speed (19 knots) was used for the plot in Figure 34.

The optimal resistance solution (number 1049) blister cost, hull form total resistance and SPI are shown in Table 8 and the hull form is shown in Figures 35 and 36.

Table 8: Comparison of optimal resistance solution (number 1049) to the baseline hull characteristics

	Baseline 5415	**Solution 1049**	**Solution 1049 No Bulb**
Blister cost	N/A	$5.469M	$5.469M
Resistance at 15 kts	2.262E5 N	2.286E5 N	2.274E5 N
Resistance at 17 kts	3.177E5 N	3.047E5 N	3.049E5 N
Resistance at 19 kts	3.904E5 N	3.851E5 N	3.856E5 N
SPI	0.61296	0.66247	0.66247
Prop. fuel expense	$6.062M	$6.166M	$6.135M

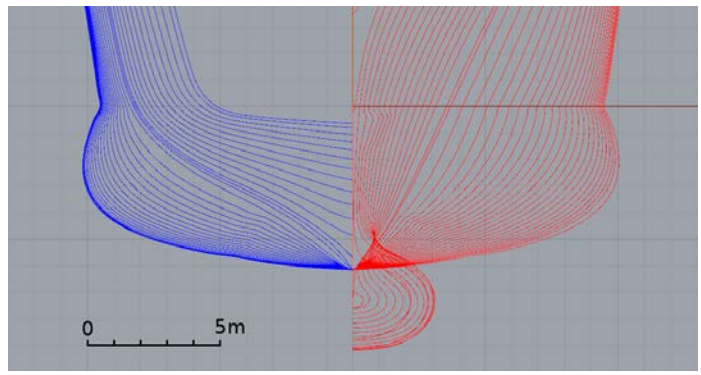

Fig. 35 Optimal resistance solution (number 1049) body plan. Red lines on the right define the form forward of midships and the blue lines in the left define the aft region

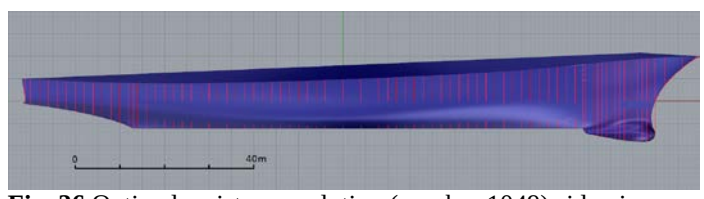

Fig. 36 Optimal resistance solution (number 1049) side view

Figure 35 shows the hull solution 1049 in body plan form. Red lines on the right define the form forward of midships and the blue lines in the left define the aft region. Lines do not strictly adhere to stations, and derive from the offset file, with lines placed more closely in areas of rapid geometric change. A bow bulb does exist just below the waterline, but its size is modest. Figure 36 shows the baseline DTMB-5415 hull form in blue and the modified hull lines in red (from 'inside' the hull). The two designs match where the modified hull lines intersect with the baseline hull form. The breaks in the red lines define the region where the blister and bulb surfaces diverge from the baseline hull.

The total resistance for hull solution 1049 at 19 knots shown in Table 8 is approximately 1.4% less than the baseline hull. Note that the total resistance at 15 knots is 1.1% higher than that of

the baseline hull. This type of situation, where not all goals are improved over a baseline target, can be due to an objective function's formulation. In this case the hull resistance values are naturally weighted toward the higher speed values; improvements made at higher speeds can more than compensate for deficits at the lower speeds. Changing the hull resistance objective function to more heavily weight the lower speed values, or splitting the function up into three separate values to be optimized are alternative formulations, depending on the goals of the design optimization problem.

The estimated annual propulsion fuel expense for this hull design is only slightly greater than that of the baseline hull; an increase of 1.7%. Given the minor increase to the operational fuel expense, the benefit of having the additional displacement is limited to the cost of the blister.

The 1049 solution without the bow bulb was also analyzed for hydrodynamic performance and cost. The blister modification cost and seakeeping performance are unchanged. The hull resistance performance is nearly unchanged, except at operational speeds lower and higher than those used for the optimization. For this hull form, the bulb is more beneficial at the higher speeds, and less beneficial at the lower speeds. The modest benefit of not having a bulb at lower speeds shows in the slight improvement in propulsion fuel expense, being reduced by $31k annually.

The optimal blister cost solution (number 2850) blister cost, hull form total resistance and SPI are shown in Table 9 and the hull form is shown in Figures 37 and 38.

Table 9: Comparison of optimal blister cost solution number 2850 to the baseline hull characteristics

	Baseline 5415	**Solution 2850**	**Solution 2850 No Bulb**
Blister cost	N/A	$4.308M	$4.308M
Resistance at 15 kts	2.262E5 N	2.315E5 N	2.277E5 N
Resistance at 17 kts	3.177E5 N	3.327E5 N	3.328E5 N
Resistance at 19 kts	3.904E5 N	4.288E5 N	4.281E5 N
SPI	0.61296	0.65287	0.65287
Prop. fuel expense	$6.062M	$6.475M	$6.398M

As shown in Table 9, the total resistance for hull solution 2850 at all three speeds of the objective function are higher than for the baseline hull. A bow bulb does exist just below the waterline and its size is more prominent than that of solution number 1049. Comparing the solutions in Figures 36 and 37, it can be seen that solution 2850, with the lower blister cost, has the blister distributed over a shorter length of the hull. The blister and bulb for this solution displaces the same volume as for solution 1049, but does it in a more geometrically efficient manner, requiring less surface area and structure, and ultimately costs less to construct. However, this geometry is less efficient with respect to calm water resistance.

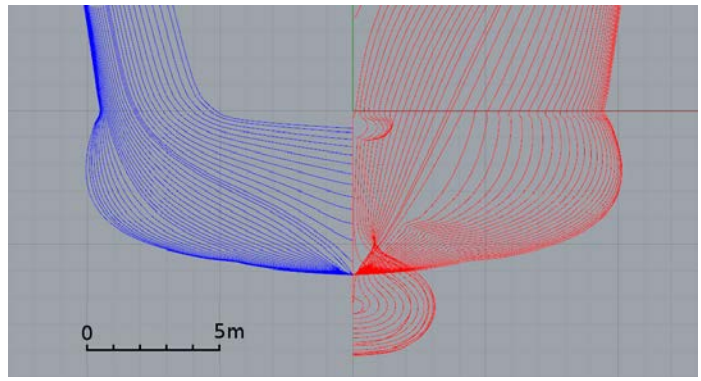

Fig. 37 Optimal blister cost solution (number 2850) body plan. Red lines on the right define the form forward of midships and the blue lines in the left define the aft region

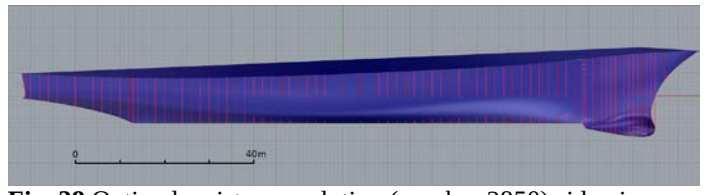

Fig. 38 Optimal resistance solution (number 2850) side view

The estimated annual propulsion fuel expense for this hull design 6.8% greater than that of the baseline hull. However, the cost of this blister is $1.16M less expensive the version on solution 1049.

The 2850 solution without the bow bulb was also analyzed for hydrodynamic performance and cost. The blister modification cost and seakeeping performance are unchanged. The hull resistance performance is nearly unchanged, except at operational speeds lower and higher than those used for the optimization. For this hull form, as with solution 1049, the bulb is more beneficial at the higher speeds, and less beneficial at the lower speeds. The benefit of not having a bulb at lower speeds shows in the improvement in propulsion fuel expense, dropping from $6.475M to $6.398M annually.

In summary, it can be seen that a variety of intriguing and potentially feasible design trade-off solutions can be obtained in a relatively short period of time, given the challenging goals and constraints. These solutions should be further investigated and refined using high fidelity tools.

This design problem was formulated as an all-at-once optimization (blister and bulb variables modified all-at-once), but it could be further enhanced by adding a second optimization loop, refining the bulb's hydrodynamic contribution for each given hull blister design. Given the impact on annual propulsion related fuel expenses, the optimization should consider hull performance at the lower speeds as well as the higher speeds.

Using the offset file formulation for the hull presents some limitations to the types of geometry that may be represented.

The bow bulb generated for this optimization analysis was relatively constrained in its position in order to adhere to traditional hull offset file formulation.

4.3 Solution Comparison

Two different methods were utilized to determine an improved solution constrained to have a hull blister of a given volume. The following figures and tables attempt to quantify these differences. Figures 39 and 40 compares the geometry between solutions generated by manual geometry manipulation and a RANS solver to that generated by automated geometry manipulation and potential theory solvers. Table 10 shows the results of using MHTRES and SHIPMO to analyze the Iowa hull form.

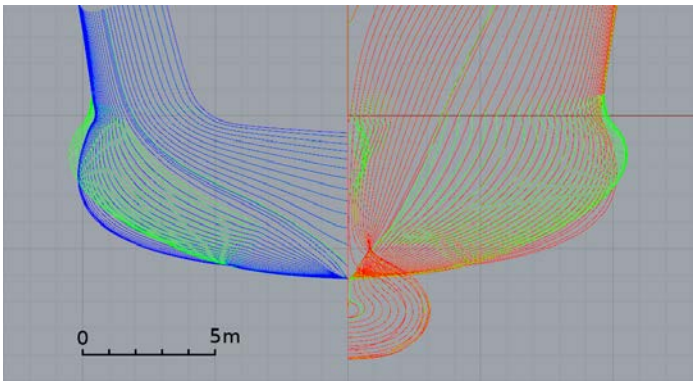

Fig. 39 Optimal resistance solution (number 1049) body plan drawn in red and blue compared with the optimal Iowa solution, drawn in green

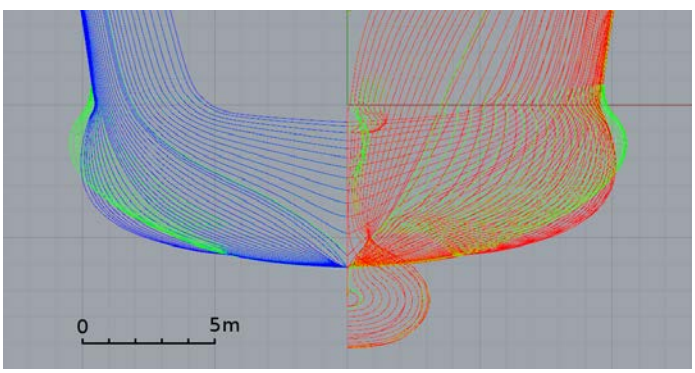

Fig. 40 Optimal blister cost solution (number 2850) body plan drawn in red and blue compared with the optimal Iowa solution, drawn in green

The results in Table 10 indicate that the Iowa solution has hull total resistance values close to that of the baseline hull, with those at 15 and 19 knots being slightly above and resistance at 17 knots being slightly below. The SPI value is an improvement over the baseline, but the value is not as high as either solution 1049 or 2850.

Table 10: Comparison of Iowa solution to the baseline hull characteristics using potential theory tools MHTRES and SHIPMO

	Baseline 5415	**Solution Iowa**
Blister cost	N/A	$5.650M
Resistance at 15 kts	2.262E5 N	2.307E5 N
Resistance at 17 kts	3.177E5 N	3.151E5 N
Resistance at 19 kts	3.904E5 N	3.982E5 N
SPI	0.61296	0.63074
Prop. fuel expense	$5.456M	$6.294M

The estimated annual propulsion fuel expense is higher than the baseline value, which is a different result than obtained by the computations performed using CFDShip. The MHTRES analysis indicates that the Iowa solution has higher total drag than the baseline hull form for the speeds not used for the optimization, both higher and lower.

4.4 MHTRES Solver Validation

Prior to using MHTRES for this analysis its results were validated against an experimental data of the DTMB-5512 model hull (Gui et al, 2001, and Longo and Stern, 2005), as shown in Figure 41. MHTRES results are quite close to experimental data between Froude numbers 0.17 and 0.37, and diverge somewhat higher outside these bounds.

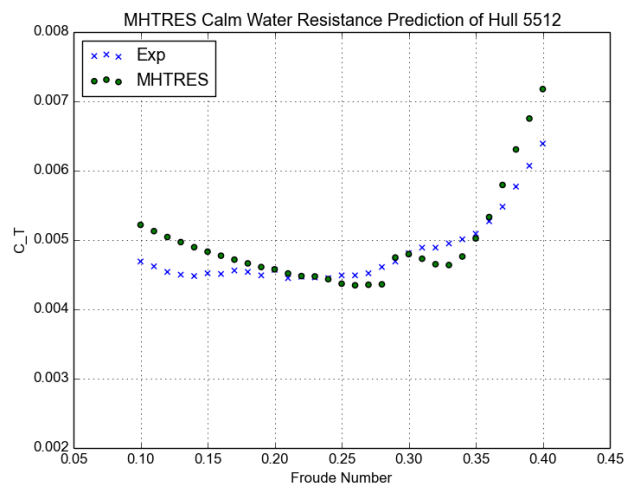

Fig. 41 Comparison of MHTRES and experimental results of total calm water resistance coefficient for the DTMB-5512 hull (Gui, L. et al, 2001, and Longo, J. and Stern, F. 2005)

The full-scale speeds of interest are 15 to 19 knots, which correspond to Froude numbers 0.22 to 0.27. As can be observed from the plot, MHTRES agrees closely with the experimental data in this speed range.

Given that MHTRES does trend above the experimental data outside Froude numbers 0.17 to 0.37, it may explain why predicted full scale resistance and fuel costs are not reduced as much as expected in those speed ranges for optimized solutions,

as compared to the solution generated by CFDShip.

5. STRUCTURAL ANALYSIS

Structural analyses of the hull modification redesigns were performed using the finite analysis code, ABAQUS (Abaqus 6.13, 2013). Structural hull forms similar to the baselineDDG-51 DTMB-5415 are available. The initial effort was to use these structural details for development of finite element analyses of the representative structural hull with and without the blister modifications. The models without the blister were first subject to a preliminary validation by comparison of the results with previous analyses. Then, these finite element models were modified to include initial designs of the blister using preliminary structural stiffener designs. Further refinements in the details of the model and structural design of the blister, including discrete modeling of the blister stiffening designs were then developed. These results showed a need for further refinement on the hull-blister interface when using the blister geometry found from hydrodynamic performances optimization. Efforts for arriving at a proposed structural design of the blister, including the use of composite components at the interface of the shells, follow.

5.1 Initial CAD and FEM Modeling

The DDG-51 DTMB-5415 representative structural modelhull section located 38.4 m to 53.0 m, aft of FP and bulkhead to bulkhead, was selected as a representative section of the vessel for finite element analysis and to study the details for the addition of the composite side blisters. The section is encircled in Figure 42. The structural details of the DDG-51 DTMB-5415 representative are given from the data bank of the ASSET Program (NSWC, ASSET, 1990). The section is referred to in ASSET as Section 07, the numbering scheme begins at the bow with Section 01.

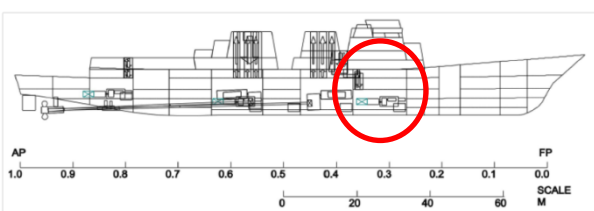

Fig. 42 Hull Structure Section

A cross section of the hull, decks and stiffeners is shown in Figure 43. The area centroid is located along the vertical centerline, 6.76 m above the keel (6.01 m below the top deck). The length of the section is L = 14.6 m.

The structural details from ASSET were then used to develop CAD models using Rhino 5 [Rhinoceros, 2014]. A Rhino STEP 3D CAD model can then be read by the finite element general purpose program ABAQUS. The Rhino model for section 07 was translated to ABAQUS directly (ABAQUS reads the Rhino model file extension .stp). A partial view of the ABAQUS FEM model is shown in Figure 44.

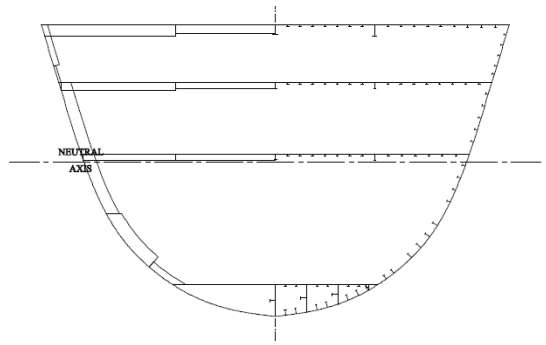

Fig. 43 Hull Representative Cross Section

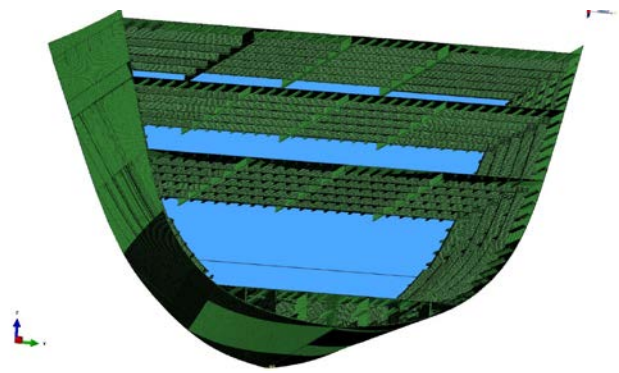

Fig. 44 ABAQUS FEM image of the selected section (looking forward).

To provide an initial effort for verification of the FEM model, the aft boundary of the section was fixed in space. Also, to compare the FEM results with beam theory, we provide a rigid (but moveable) plane at the forward end of the section (the shaded blue plane in the figure). The intent is to represent the constraint offered by the remaining forward portion of vessel. This constraint is thus consistent with primary beam bending theory in which plane cross sections remain plane.

Our initial comparison is to consider the sagging design moment, M = 36,024 m-Mton. The midship moment of inertia is given in ASSET as I = 226,545 m^2cm^2. The beam theory (ASSET) stress level at the deck is then 105.5 MPa and at the keel is -93.67 MPa. Also from beam theory, with one end fixed and the other end free to rotate, the applied sagging design moment yields a rotation of 1.1 x 10^{-3} radians at the free end.

For the finite element analysis, a rotation angle of the same magnitude is applied at the free end which yields a deck stress of -88.9 Mpa and keel stress of 111 Mpa. These values were taken from the center of the length of the section. The deck and keel stresses varied with length and increased at the ends; this deviation from beam theory is attributed to 3D effects of the end constraint. The resulting bending moment implied by this rotation is approximately 34,094 m-Mton.

A summary table is provided below (Table 11). At this point, we constrained displacements completely at the fixed end and allowed only a rotation of the cross sectional plane at the other end. The FEM analysis is of course 3D and thus this constraint does not allow for any deflections attributed to Poison effects. Such effects are not constrained in beam theory, that is, displacements within the plane of the cross section are permissible. Another source of differences between the two models is the relatively short length to depth ratio of our beam segment. This would imply amplification of the end effects in comparison to 1D beam theory.

Table 11: Summary of Bending Stress Analyses from Beam Theory and 3D FEM Analysis

Analysis Type	Applied End Rotation (rad.)	Resulting Sagging Moment (m-MTon)	Bending Stresses (MPa)	
			Keel	Deck
Beam Theory 1D	0.0011	36,024	105	-93.7
Finite Element 3D	0.0011	34,094	111	-88.9

5.2 FEM Blister Modeling

The same hull section has also been re-modeled to include the blister modifications. The first step was to reduce the number of degrees of freedom of the finite element model of the baseline hull section. The model described in the previous section resulting from our CAD-to-FEM translation was extremely large, taking hours to run on ABAQUS, quite unsuitable for design purposes. This remodeling effort reduces run times to minutes rather than hours. Shown in Figure 45 is the revised model without the blister.

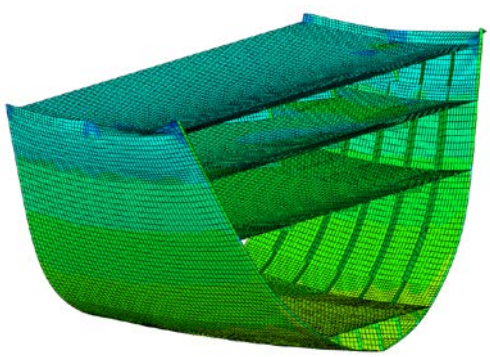

Fig. 45 ABAQUS Revised FEM image of the selected section.

The model uses effective thicknesses for the hull based on smeared properties of the longitudinal stiffeners. To test the model we again applied a rotation of 1.1 x 10^{-3} radians at the free end. This is similar forcing used for the previous model with the same boundary conditions. For a hogging moment, we found deck stresses of 112 Mpa for the new model compared to 105 Mpa for the CAD based FEM. The maximum stresses in the keel and deck for the two models were within approximately 5 and 6 % respectively. These results are quite consistent with the previous findings from beam theory and the CAD based FEM modeling.

Our next effort was to then add the blister section to the revised model. Figure 46 provides an image of the loaded condition under sagging moment of section 7 with the blister attached. The blister material is steel with an equivalent thickness of 15 cm based on our first estimates of the blisters' stiffening. These analyses produced results for the axial stress values of section 7 with loading conditions repeated from those with the new model without the blisters.

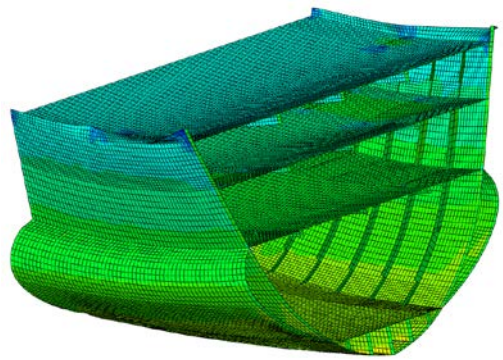

Fig. 46 ABAQUS FEM image of the section with preliminary blister design

Table 12: Summary of Bending Stress Analyses from FEM Analyses with and without the Blisters

Stress Values		
	Without Blister	**With Blister**
σ_{Deck} **[MPa]**	-121.26	-119.67
σ_{Keel} **[MPa]**	96.9	82.49
$\sigma_{Blister}$ **[MPa]**	-	80.77

Table 12 provides the average stress at the deck and the average stress at the keel, with and without the blister. The maximum axial stress of the blister is also provided in Table 12. The applied sagging bending moment was 3.53×10^9 Nm.

5.3 Structural Redesign CAD and FEM Modeling

Further steps in our structural analyses were conducted on the section 7 model with the attached blisters for two different loading scenarios. The first load case was the sagging bending moment of 3.53×10^9 Nm. This provides a direct comparison of the changes in stress levels resulting from the addition of the blister.

The second load case considers a moment of 3.82×10^9 Nm and a pressure of 82,280 Pa applied to the blister and bottom shell. This moment represents an increase of 8% from the initial

design primary bending moment. This additional moment was considered to account for an estimated increase in payload which would cause an increase in primary bending design moments. Also, the applied pressure is equal to the average pressure acting on the hull below the water line. The pressures were taken from the hydrodynamic analyses discussed in the previous section for the new blister geometry. The summary of the axial stress results from these analyses are provided in Table 13.

Table 13: Blister Model Axial Stress Comparisons

Blister Model Axial Stress				
		Initial	Modified	% Increase
Moment	[Nm]	3.53E+09	3.82E+09	-
Pressure	[Pa]	0	82280	-
σ_{Deck}	[MPa]	-119.67	-130.75	9.26
σ_{Keel}	[MPa]	82.49	89.51	8.51
$\sigma_{Blister,Max}$	[MPa]	80.77	90.78	12.39

The next effort in the structural redesign involved remodeling the same hull section and blister with discrete stiffening in the transverse and longitudinal directions, representing transverse frames and longitudinal stiffeners. This allows for the examination of the local stresses in the plating. Figure 47 provides an image of the new CAD model used in the analyses. This model was then translated to an ABAQUS finite element model as previously described. It is noted that the structural details include new discrete stiffener designs in the blister while maintaining the stiffening arrangements in the main hull.

The analyses described in the previous section are repeated with the applied design bending moment, with and without external pressure. A list of maximum Von Mises effective stresses is shown in Table 14. The results indicated some increase in stresses as expected.

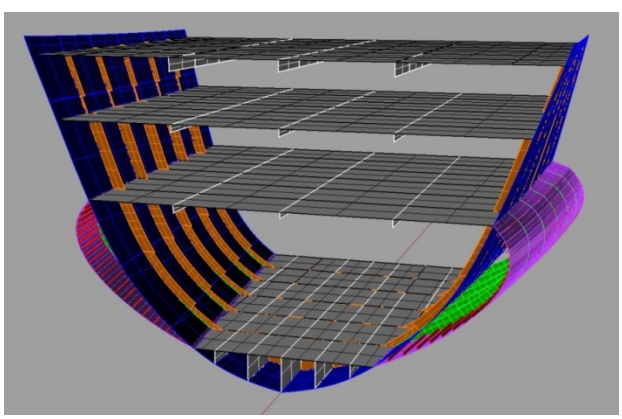

Fig. 47 Rhino image of the section 7 with revised blister design and discrete stiffening

Of particular note was a considerable increase in stresses near the top and bottom of the blister. An example result is shown in Figure 48. Location 1 is a transverse slice of the blister outer shell located midway between the forward transverse bulkhead and the next frame aft. Location 1 is thus 39.6 m aft of FP. This location can be seen in Figure 47 which shows the hull and blister stiffening just aft of the transverse bulkhead. The nodes start at the bottom of the blister and increase in the upward direction, with nodes at each longitudinal stiffener and midway between each longitudinal stiffener.

Table 14: Blister Discrete Stiffener Model Von Mises Stress Comparisons at Location 1

Section 7 Stress Values		
Model:	Blister with Internal Structure	
	Bending Moment:3.82E+09 [Nm] Pressure: 0 [Pa]	Bending Moment:3.82E+09 [Nm] Pressure: 82280 [Pa]
Deck Stress [MPa]	121.36	122.97
Keel Stress [MPa]	102.03	104.82
Max. Blister Stress [MPa]	92.42	163.91

Considerable stress increases at the bottom of the blister shell are noted, peaking at 163.9 MPa in this location. Similar increases result at all locations along the length of the section; these results needed further examination. It is noted that the model was based on the current stiffener design; there was no modification of the parent hull.

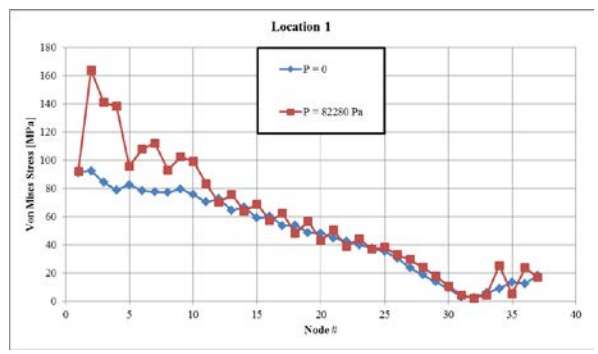

Fig. 48 ABAQUS FEM results for discrete stiffening, M = 3.82×10^9 Nm, P = 0 and 82280 Pa

Further effort therefore involved the development of revised models for analyzing the interface between the blister and hull walls. The peak stresses for the combined bending and pressure loading conditions were found to be due to local bending (tertiary) stresses. This is a result of maintaining the hull design and thus no stiffening was provided at the interface of the shell walls.

Our next redesign effort was then to examine the effects of providing a longitudinal stiffener at the interface location. This substantially reduced the troublesome stress peaks at these points. The stiffener was added to the hull with the same geometry and properties as the other longitudinals in that region. The stress results are shown for Location 1, in Figure 49, for three conditions: no hydrostatic pressure, hydrostatic pressure with no stiffening at the hull-blister interface, and the new results for hydrostatic pressure with a longitudinal stiffener

added along the bottom of the blister. Similar behavior is shown in Figure 50 for Location 2 which is midway between the first and second transverse frames of the section. Table 15 lists the peak stresses at each of 6 transverse locations with and without hydrostatic pressure. The stresses which include pressure are results for the newer model with a longitudinal stiffened added to the hull at the blister interface.

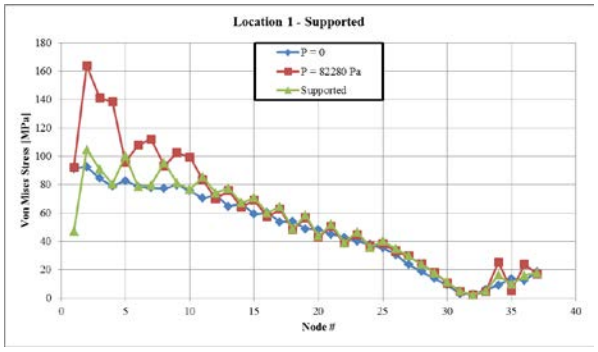

Fig. 49 ABAQUS FEM results for discrete stiffening, M = 3.82×10^9 Nm, P = 0 and 82280 Pa. Longitudinal stiffening provided at lower hull/blister interface. Location 1 is 39.6 m aft of FP

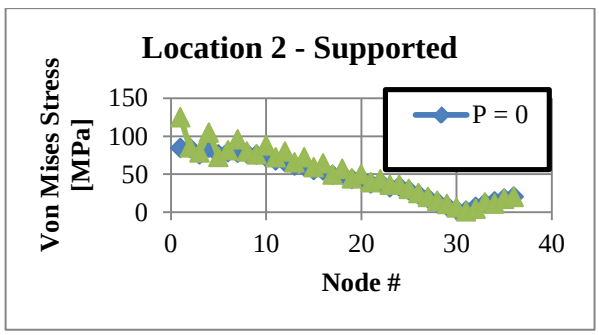

Fig. 50 ABAQUS FEM results for discrete stiffening, M = 3.82×10^9 Nm, P = 0 and 82280 Pa. Longitudinal stiffening provided at lower hull/blister interface. Location 2 is 42.1 m aft of FP

Table 15: Blister Discrete Stiffener Model Von Mises Stress Comparisons at Locations 1 – 6. Longitudinal stiffening provided at hull-blister interface

Maximum Von Mises Stress

Location	Von Mises[MPa]		% Increase
	P = 0 Pa	P = 82280 Pa	
1	92.4	104.5	13.1
2	84.7	125.0	47.6
3	88.2	100.5	13.9
4	75.8	90.9	20.0
5	73.2	91.3	24.7
6	71.4	90.7	27.0

5.4 Refinement of Hull/Blister Interface Design

At this stage of iterations on the structural redesign for the blister modifications, both revised blister geometry and external pressures were used in the finite element models. Also, the study of the interface stresses to this point involved simply adding a longitudinal to the hull at the interface; this allowed us to quickly establish the need for some reinforcement in this area.

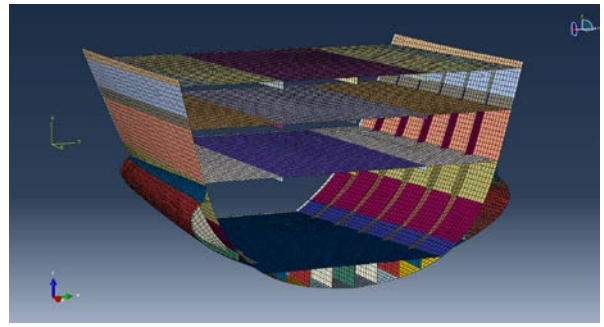

Fig. 51 Hull Structure Section 07: ABAQUS with new blister geometry.

However it is preferable to have such stiffening located in the blister design rather than a hull modification. The further modifications to the blister involved an E-glass composite section in the interface region, shown in blue along the uppermost blister segment of Figure 51. Further detail of the blister plating and stiffening schematic is depicted in Figure 52.

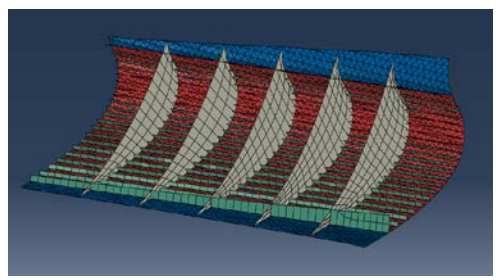

Fig. 52 New blister modifications: ABAQUS model details.

Composite material is shown in blue along the top and bottom of the blister in the figure. Materials engineering and physical properties are provided in Table 16. The finite element analysis results for the global hull girder bending analysis, for comparison with our preliminary results of Table 11, are shown in Table 17. Peak blister stresses have been considerably reduced from the high values of the unsupported interface design (Figures 48 and 49) by the redesign with composite interface segments.

Table 16: Blister Properties

	MATERIAL	YOUNG'S MODULUS	POISSON'S RATIO	DENSITY	THICKNESS
BLISTER SHELL	A36 Steel	204.085 GPa	0.3	7850 kg/m^3	6 cm
BLISTER SHELL COMPOSITE	E-Glass	70.00 GPa	0.21	2550 kg/m^3	5 cm
BLISTER WEBS	A36 Steel	204.085 GPa	0.3	7850 kg/m^3	6 cm
BLISTER STIFFENERS	A36 Steel	204.085 GPa	0.3	7850 kg/m^3	6 cm

Table 17: Summary of Bending Stress Analyses from Beam Theory and 3D FEM Analysis

	Model Without Blister	Model With Blister	Model With Blister (composite edges)
σ_{Deck} [MPa]	-111.40	-115.33	-115.16
σ_{Keel} [MPa]	101.68	96.76	97.89
$\sigma_{Blister}$ [MPa]	-	64.40	58.25

5.5 Structural Redesign Summary and Future Efforts

The two new design load cases involving consideration of increased hull girder bending moments and hydrostatic pressure can be well accommodated by the blister design. In fact, the peak stresses resulting in the hull with the addition of the blister and increased global bending moment are very similar in magnitude in comparison to the original steel hull design stress levels. This does require however careful attention to the details of the interface of the blister and hull shells, particularly the local geometry and stiffness. Note also that the geometry of the blister which results from an optimization of the hydrodynamics of the vessels is used. No compromise of this optimization is made for the structural detailing. Further analyses for examining local details of the fastening schemes for the blister are required (see Shkolnikov, 2014), and are beyond the scope of this paper.

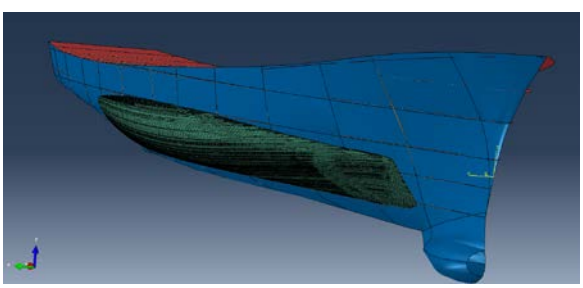

Fig. 53 Blister modifications for multiple hull sections of the DDG51 DTMB 5415.

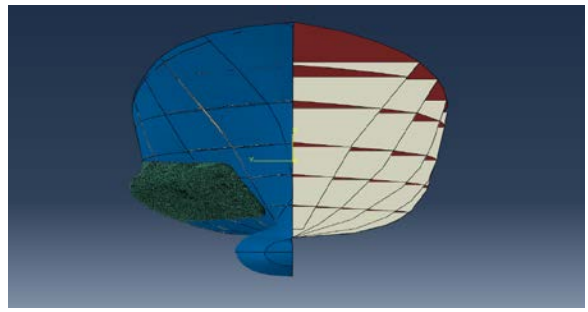

Fig. 54 Blister modifications for multiple hull sections of the DDG51 DTMB 5415.

Our structural analyses were conducted using the available structural details due to the very close similarity with the DDG-51 DTMB-5415 and the availability of that geometry in various formats including ASSET. Also our structural redesign was focused on one key section of the hull. Redesign efforts are also needed using the DDG-51DTMB-5415 geometry with extended portions of the vessel. To this end, for example, new ABAQUS finite element models (Figures 53 and 54) are under development for multiple sections of the hull and are the subject of on-going study.

6. CONCLUSIONS

High-fidelity URANS simulation based design tools that have previously been successfully implemented for a variety of design optimization problems were used to design and investigate the hybrid ship concept designs that could accommodate an increase in displacement with minimum resistance and cost penalties. A shoulder wave cancellation mechanism was identified, which allowed for progressive analysis of geometry variations for the best blister design variables capable of producing destructive interference of the diverging Kelvin wave over the design speed range. The results indicated that a reduced resistance was possible even with an increase in displacement through shape optimization of the blister for shoulder wave cancellation. In addition, the blister improved the sea-keeping characteristics due to viscous damping of the pitch, heave, and roll motions. A bow-bulb was also designed based on previous studies by Cusanelli and Karafiath (2012), and the blister design variables were tuned to account for the flow modification induced by the bow bulb.

In calm water conditions, the 5415 w/ bow bulb alone shows a resistance reduction of ~8% *w.r.t.* the baseline 5415 in the design speed range of 15-19 knots, even though the displacement is increased by 5%, such that the transport factor is increased by 13%. The 5415 w/ both blister and bow bulb shows a resistance reduction of ~11% *w.r.t.* the baseline 5415 in the design speed range of 15-19 knots, even though the displacement is increased by 8%, such that the transport factor is increased by 19%. However, the blister increases the resistance in the off-design speed ranges; so that the annual cost of operation based on the current speed time profile for the 5415 w/ bow-bulb alone is less than that of 5415 w/ combined blister and bow-bulb. In summary, for an additional 5% payload on the

deck, the estimated annual cost of operation for 5415 w/ bulb alone shows a 6.2% reduction *w.r.t.* the baseline 5415; the estimated annual cost of operation for 5415 w/ blister and bulb shows a 5.8% reduction *w.r.t.* the baseline 5415.

Lower fidelity multi-criterion hydrodynamic optimization using MHTRES with sea-keeping performance measurements provided three set of trade-off hull solutions for blister costs and sea keeping performance indexes. A blistered hull solution with a low blister cost of $4.64 M and an improved SPI of 0.8439 over the original hull was pursued and recommended for follow-on study. However, evaluation of the URANS based optimized bulb and blister design using MHTRES gave conflicting results, with the resistance of the optimized hull being greater than the baseline; and contrary to the MHTRES solutions, the URANS solutions do not indicate a resistance reduction for the thin-ship theory based optimized geometry. Further investigation is required to validate and correlate thin-ship theory codes with higher fidelity codes for complimentary use in design optimization analyses.

Three-dimensional finite element modeling and structural analyses of hull models with and without blister modifications involving consideration of increased hull bending moments and blister hydrostatic pressure concluded that the blistered hull design can be accommodated, suggesting the use of E-glass composite interface treatments at the top and bottom of the blister and the parent hull shells to reduce peak blister stresses and maintain minimal change to the hull global bending stresses.

Future plans include resistance and sea-keeping calculations of the optimized geometry *5415BLB8* in oblique waves at sea-state 4 using both the higher fidelity and lower fidelity codes. The lower fidelity sea-keeping code will be validated using 5415 experimental data and correlated with the high fidelity code. For the structural part, further analyses are recommended for examination of local joint connections of the blister to the hull. The optimized geometry *5415BLB8* should be model tested and validated in both calm and rough waters.

ACKNOWLEDGEMENTS

The present research is supported by the Office of Naval Research, Grant #N000141110237 and #N000141010529, under the administration of Dr. Roshdy Barsoum. The URANS computations were performed at the NAVY DoD Supercomputing Resource Center. The authors would to acknowledge the contributions to project from Jinfu He, Matthew Lankowski, Kurt Nielson, Nan Si, Andrew Stankovich, Eileen Tausch, Dave Ruley, Michael Goodman, and Brandon Laing.

REFERENCES

Anderson, T., Gerhard, K., Sievenpiper, B., “Operational Ship Utilization Modeling of the DDG 51 Class”, In Proceedings ASNE Day 2013, pp. 303-306, Arlington, Virginia, USA, 21-22 February, 2013.

Abaqus 6.13 Documentation. Simulia, Dassault Systemes, 2013.

Barsoum, R.G.S., 2013, "Hybrid composite and metallic hulls, the best of both worlds," Analysis and Design of Marine Structures, CRC Press

Barsoum, R.G.S., Hybrid Ship Hull, US patent 6,941,888, Sept. 13, 2005

Beck, R. F. and Troesch, A. W., “SHIPMO.BM Users’s Manual”, University of Michigan, Department of Naval Architecture and Marine Engineering, Report No. 89-2, pp. 48, 1989.

Campana E.F., Peri D., Pinto A., Tahara Y. and Stern F., “Shape Optimization in Ship Hydrodynamics using Computational Fluid Dynamics”, Computer Methods in Applied Mechanics and Engineering, Vol. 196, 634-651, 2006.

Campana E.F., Peri D., Kandasamy M., Tahara Y. and Stern F., “Numerical Optimization Methods for Ship Hydrodynamic Design”, SNAME annual meeting, Providence (Rhode Island, USA), 2009.

Cusanelli, D.S., “Performance of Near-Surface Bow Bulbs in Irregular Waves,” 25th ATTC, Iowa City, IA (Sept 1998).

Cusanelli, D.S. and Karafiath, G., “Hydrodynamic Energy Savings Enhancements for DDG 51 Class Ships,” *Naval Engineers Journal*. 2012;124(2):123–38.

Doctors, L.J., “Near-Field Hydrodynamics of a Surface-Effect Ship,” Journal of Ship Research, Vol. 56(3), pp. 183-196, September 2012.

Hibbett, Karlsson, and Sorensen. *ABAQUS/standard: User's Manual*. Vol. 1. Hibbitt, Karlsson & Sorensen, 1998.

Huang, J., Carrica, P.M., and Stern, F., “Semi-Coupled Air/Water Immersed Boundary Approach for Curvilinear Dynamic Overset Grids with Application to Ship Hydrodynamics,” International Journal Numerical Methods Fluids, 58, 6, pp. 591–624, 2008.

Kandasamy M., Keat Ooi S., Carrica P. and Stern F., “Integral Force/Moment Waterjet Model for *CFD* Simulations”, Journal of Fluid Engineering, 2010, Vol. 132, No 10.

Kandasamy, M., Peri, D., Tahara, Y., Wilson, W., Miozzi, M., Svetlozar, G., Evgeni, M., Campana, E., and Stern, F., “Simulations based design optimization of waterjet propelled Delft catamaran,” International Ship Building Progress, Invited paper, Vol. 60, No.1, pp. 277–308, 2013.

Keane, R. G., and Sandberg, W. C., "Naval Architecture for Combatants, a Technology Survey", Naval Engineers Journal, Vol. 92, 47-64, 1984.

Lewis, E. V., "Principles of Naval Architecture," Society of Naval Architects and Marine Engineers, Volume 3, 1989.

Mitchell, J. H., "The Wave Resistance of a Ship," Philosophical Magazine, Series 5, Vol. 45(272), pp. 106-123, January, 1898.

Naval Sea Systems Command. (2012, August). Calculation of Surface Ship Annual Energy Usage, Annual Energy Cost, and Fully Burdened Cost of Energy, DDS 200-2

NSWC, ASSET " User Manual", Version- 5.0, David Taylor Model Basin, Carderock Division, Naval Surface Warfare Center, May 1990.

Rhinoceros, Rhino 5, http://www.rhino3d.com. , 2014.

Robert McNeel & Associates. Rhinoceros User'sGuide 2002; Ver 3.0: 146-149, 2002.

Salveson N., Tuck, E. O., and Faltinsen, O., "Ship Motions and Sea Loads," Society of Naval Architects and Marine Engineers Transactions, Vol. 78, pp. 250-287, 1970.

Shkolnikov, V. M. *Hybrid Ship Hulls: Engineering Design Rationales*. Elsevier Science, 2014.

Tahara Y., Peri D., Campana E.F. and Stern F. "*CFD*-Based Multi-Objective Optimization of a Surface Combatant by Using Global Optimization Method", Journal of Marine Science and Technology, N.13, pp 95-116, 2008.

Vandroff, Mark, CAPT (USN) (2013). DDG-51 Update. Presentation at Surface Navy Association 2013, Arlington, VA. Retrieved from : http://www.navsea.navy.mil/Media/SNA2013/DDG51%20UPDATE%20(CAPT%20Vandroff)%20-%20FINAL.pptx

Zalek, S. F., Parsons, M. G., and Beck, R. F., "Naval Hull Form Multicriterion Hydrodynamic Optimization for the Conceptual Design Phase", Journal of Ship Research, Vol. 53(4), p.1-15, 2009.